Electronic Supplementary Information (ESI) for

Super-Stretchable and Extreme Temperature-Tolerant Supramolecular-Polymer Double-Network Eutectogels with Ultrafast *in situ* Adhesion and Flexible Electrochromic Behaviour

Kaifang Wang,[a,†] Hai Wang,[a,†] Jingjing Li,*[b] Yujia Liang,[a] Xiao-Qiao Xie,[a] Junpeng Liu,[a] Chaonan Gu,[a] Yunfei Zhang,[a] Guo Zhang,[a] and Chun-Sen Liu*[a]

[a] Henan Provincial Key Laboratory of Surface & Interface Science, Zhengzhou University of Light Industry, Zhengzhou 450002, China. E-mail: chunsenliu@zzuli.edu.cn.

[b] School of Chemistry and Chemical Engineering, Henan University of Technology, Zhengzhou, 450001, China. E-mail: nicoleljj@tju.edu.cn.

† These authors contributed equally to this work.

Mater. Horiz.

Table of Contents

Video S1

Simulated assembly mechanism of the BGA-12/PHEAA SP-DN eutectogel based on theoretical calculations, showing multiple hydrogen-bonding interactions within supramolecular networks and between individual supramolecular and polymer networks.

Video S2

Biaxial tension test of square BGA-12/PHEAA SP-DN eutectogel, showing over 18000% areal strain (from 2.0 × 2.0 cm^2 to 26 × 28 cm^2).

Video S3

Adhesion capacity test of the BGA-12/PHEAA SP-DN eutectogel between glass plates, which can readily sustain a 12 kg weight without detaching (Red dyes of rhodamine B were added to visually observe the SP-DN eutectogel).

Video S4

Water-resistant adhesion of the BGA-12/PHEAA SP-DN eutectogel adhesive in boiling water (100 ^oC) (Red dyes of rhodamine B were added to visually observe the SP-DN eutectogel).

Video S5

Ultra-low temperature (liquid nitrogen, –196 ^{o}C) resistant adhesion of the BGA-12/PHEAA SP-DN eutectogel adhesive (Red dyes of rhodamine B were added to visually observe the SP-DN eutectogel).

Video S6

High temperature (200 ^{o}C) resistant adhesion of the BGA-12/PHEAA SP-DN eutectogel adhesive (Red dyes of rhodamine B were added to visually observe the SP-DN eutectogel).

Video S7

Underwater *in situ* adhesion test of the BGA-12/PHEAA SP-DN eutectogel.

Video S8

Low temperature (dry ice, –80 ^{o}C) *in situ* adhesion test of the BGA-12/PHEAA SP-DN eutectogel.

Video S9

Underwater *in situ* restoration of imitation blue and white porcelain.

Section S1 Methods

1. Materials

D-(+)-gluconic acid δ-lactone (99%), 1,6-Diaminohexane (99%), 1,10-Diaminodecane (> 98%), 1,12-Diaminododecane (98%), N,N′-Methylenebis(acrylamide) (MBA, 97%) and 2-Hydroxy-4'-(2-hydroxyethoxy)-2-methylpropiophenone (Irgacure 2959, 98%) were purchased from Beijing InnoChem Science&Technology Co.,Ltd. N-(2-hydroxyethyl)acrylamide (stabilized with MEHQ, HEAA > 97.0%) was purchased from J&K Scientific Ltd. 1,1'-Dimethylferrocene (97%) was obtained from Shanghai Aladdin Biochemical Technology Co.,Ltd. Ethyl viologen diiodide (99%) was purchased from Sigma-Aldrich (Shanghai) Trading Co.,Ltd. All other chemicals used in this work were commercially analytical grade reagents without further purification.

2. Instruments

Nuclear magnetic resonance (NMR) measurements were performed on a 500 MHz NMR spectrometer (JEOL ECZ600R/S3). The chemical shift reference of ^{1}H NMR was TMS. Mass spectrometry experiments were performed on a Waters Xevo G2-XS QTof Spectrometer. Powder X-ray diffraction (PXRD) profiles were performed using a Bruker D8 Advance X-ray diffractometer using Cu Kα radiation at 25 °C. Dried eutectogel powders were obtained via solvent exchange of the wet gel by methanol followed by lyophilization. Fourier transform infrared (FT-IR) spectra of the samples were measured by Nicolet 5700 FT-IR. Circular dichroism (CD) of the eutectogels were analyzed on a Chirascan CD spectrometer. Three scans were performed from 200 to 500 nm for each sample. Carle Zeiss LSM710 confocal laser scanning microscope (CLSM) was used to observe the eutectogel morphology after being colored by fluorescein isothiocyanate (FITC). Rheological tests were performed by using a Hake Mars rheometer (Thermo Scientific) at 25 ^{o}C with a parallel plate geometry (40 mm, 0.5 mm gap). The tensile test was performed on a UTM2202 electronic universal testing machine. The compressive test and adhesion strength measurement were performed on a UTM2503 electronic universal testing machine. UV-visible spectroscopy measurement was performed using a HITACHI

UH4150 spectrophotometry. All the electrochemistry tests were measured by using the Solartron Analytical Modulab XM CHAS 08 electrochemical workstation.

3. Preparation of deep eutectic solvents (DESs)

DESs were prepared by stirring choline chloride (ChCl) and ethylene glycol (EG) in a mole ratio of 1:2 at 60 ℃ until a homogeneous solution was formed. The obtained DES was referred to as ChCl/EG (1:2). Other DESs were prepared following a similar procedure.

4. Preparation of BGA-n/PHEAA supramolecular-polymer double-network (SP-DN) eutectogels

The SP-DN eutectogels were synthesized by a simple and facile one-pot method. The composition of the SP-DN eutectogels is referred to as $(BGA\text{-}n)_x\text{-}HEAA_y\text{-}MBA_z\text{-}t$, where x is the mass of BGA-n (mg), y is the mass of HEAA (mg), z is the volume of MBA solution (μL) and t is the irradiation time (s) of the UV lamp (wavelength: 365 nm; intensity: 0.4 W cm^{-2}). The mass of Irgacure 2959 was kept at 44.8 mg, and the volume of DESs was kept at 1.0 mL. Briefly, for the synthesis of $(BGA\text{-}12)_{40}\text{-}HEAA_{1000}\text{-}MBA_{46}$-60, 40.0 mg of BGA-12 (0.072 mM), 1000.0 mg of HEAA (8.7 mM), 46 μL of aqueous MBA (10 mg mL^{-1}) and 44.8 mg of Irgacure 2959 (0.2 mM) were added to a reaction cell, followed by the addition of 1.0 mL ChCl/EG (1:2) DES. The vial was heated at 150 ℃ for 5 min to completely dissolve the mixture components. The obtained homogenous solution was then quickly poured into suitable moulds, covered with transparent glass, and cooled to RT for BGA-12 gelation. After ageing for a few minutes, the moulds were irradiated with a UV lamp with a wavelength of 365 nm and an intensity of 0.4 W cm^{-2} for ~60 s for polymerization of HEAA monomers, thus leading to the formation of the BGA-12/PHEAA SP-DN eutectogel. The irradiation time can be adjusted appropriately from 3 to 60 s according to the thickness of the sample. For example, for a tensile test sample with a thickness of 2.0 mm, less than 60 s is enough to achieve tough SP-DN eutectogels. For all adhesive specimens with a thickness of < 0.5 mm, only a 3–5 s irradiation time is required to obtain the desired adhesion strength. Other SP-DN eutectogels with different compositions were also prepared following a similar procedure to that mentioned above. The PHEAA polymer SN eutectogel was also synthesized with the same process without the addition of BGA-12. In contrast to most polymer gels that require

repeated degassing to ensure that the free radical polymerization reaction occurs, degassing in this research is not necessary during the whole process for the preparation of SP-DN eutectogels due to its high viscosity.

5. Mechanical performance characterization

Tensile and compressive test. The tensile test was carried out using a universal test machine (UTM2202) at a constant velocity of 200 mm min^{-1} in air. The sample was cut into a dumbbell-shape with the ISO 37:2011 standard size (see Figure S1 below). The compressive test was carried out using a universal test machine (UTM2503) with a 5000 N load cell at a constant velocity of 10 mm min^{-1} in air. The cylindrical eutectogels with the ISO 7743:2004 standard size (a height of 12.5 mm and a diameter of 29.0 mm) were used for compression test. To investigate the performance of the SP-DN eutectogels after undergoing different temperatures, the SP-DN eutectogels were pre-placed in a freezer with the low temperature (~ −30 ℃) and a heater (oven) with the high temperature of ~ 60 ℃ over 24 h. Then, the mechanical properties of these samples under different conditions were immediately tested after they were taken out.

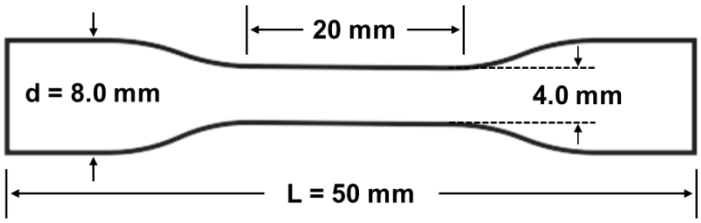

Figure S1. Geometry of tensile test samples (thickness w = 2.0 mm).

Cyclic loading-unloading test. The cyclic tensile test was performed by using the same set-up and size as the tensile test. The sample was first stretched to a fixed strain (500%) at a loading velocity of 50 mm min^{-1} followed by immediately unloading with the same speed. Without waiting, the samples were loaded for second tensile test to study their self-recovery behavior. Ten cycles in total were conducted. The dissipated energies (U_{hys}) were calculated from the area between loading-unloading curves.

Tearing test. The tearing test was performed using a universal test machine (UTM2202) in air. The sample was cut into the standard ISO 34-1:2004 1/2 sizes (50 × 15 × 2.0 mm) by using a razor blade.

The length of the initial notch is 20 mm. The two arms of the specimens were clamped with the gauge length of 10 mm, in which the lower arm was fixed, while the upper arm was pulled at a constant velocity of 100 mm min^{-1}. The tearing energy (T) is defined as the work required to tear a unit area, as estimated by[1, 2]

$$T = 2F_{av}/w$$

Where F_{av} is the average force of peak values during steady-state tear and w is the thickness of the specimen (see Figure S2).

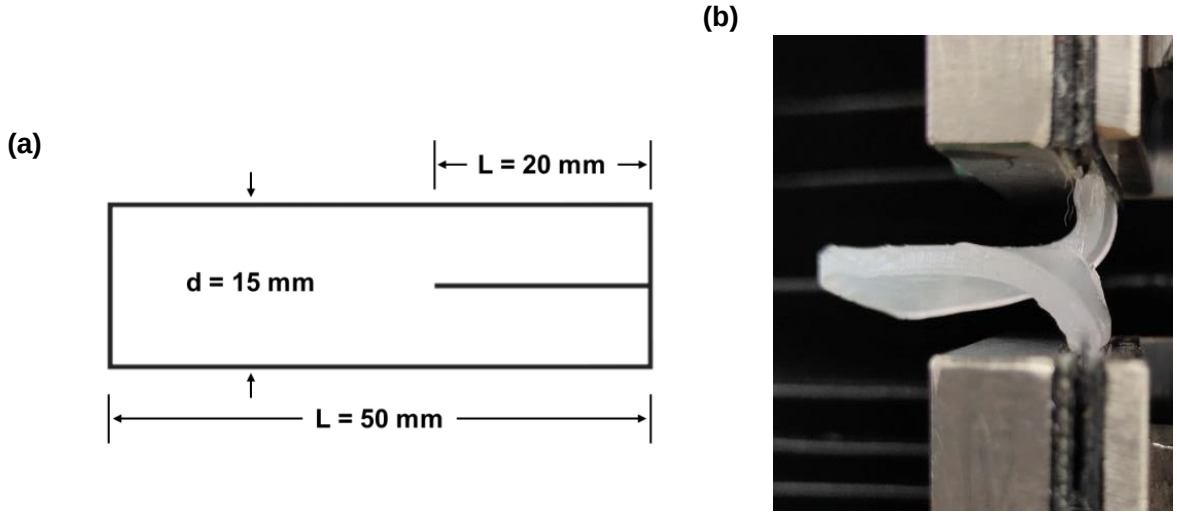

Figure S2. Tearing test to determine the tearing energy. (a) Geometry of tearing test eutectogel samples (thickness w = 2.0 mm). (b) Experimental site photo of the tearing test.

6. Adhesion test

Preparation of adhesive layers. BGA-12/PHEAA SP-DN eutectogel adhesive was prepared following a similar procedure to the bulk material as described above. Briefly, 40.0 mg of BGA-12 (0.072 mM), 1000.0 mg of HEAA (8.7 mM), 46 μL of MBA aqueous (10 mg mL^{-1}, 0.003 mM) and 44.8 mg of Irgacure 2959 (0.2 mM) were completely dissolved into 1.0 mL choline chloride/ethylene glycerol (ChCl/EG, 1:2) DES upon heating. The obtained homogenous solution was then cooled to room temperature for BGA-12 gelation. The as-prepared eutectogel samples were pipetted on different substrates including hydrophilic glass, wood and various metal plates, as well as hydrophobic polyethylene terephthalate (PET), poly(methyl methacrylate) (PMMA) and polytetrafluoroethylene

(PTFE). And then a new glass substrate was covered on the coating layer. After *in situ* photopolymerization under the irradiation of a UV lamp (365 nm, 0.4 W cm^{-2}) for ~5 s, the two plates adhered immediately and firmly together (see Figure S3 below). After the excess gel that was squeezed out and trimmed, the adhered plates were further used for lap-shear and macroscopic test. The lap-shear test was also performed on a UTM2503 electronic universal testing machine with a pull rate of 500 mm s^{-1} (each adhesion test was carried out for at least three times in parallel). For each test, the amount of adhesive coated on surfaces was around 3−4 mg cm^{-2}.

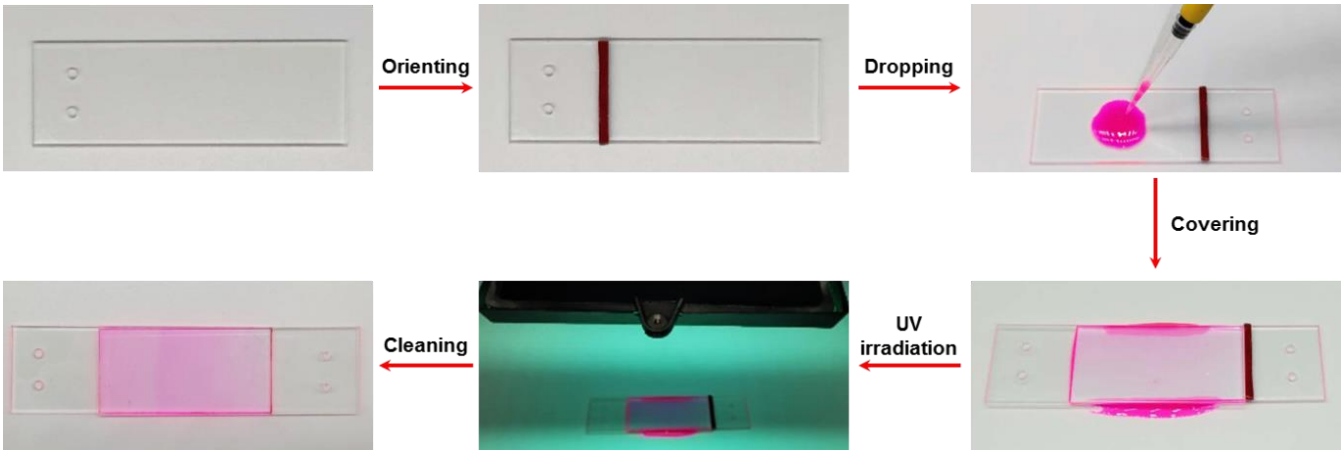

Figure S3. Fabrication process of BGA-12/PHEAA SP-DN eutectogel adhesive layers between glass plates. Red dyes of rhodamine B were added to visually observe the SP-DN eutectogel.

Solvent-resistant and temperature-resistant adhesion tests. The fabrication of adhesive layers were the same as the solvent-free process. Before testing, the adhered plates were totally immersed in different solvents for at least 24 h for solvent-resistant adhesion test and were placed in liquid nitrogen (–196 ^{o}C) over 1 h (See Video S6) or an oven (200 ^{o}C) for at least 12 h (See Video S7) for temperature-resistant adhesion test.

Underwater and ultra-low temperature in situ adhesion tests. The preparations of the adhesive layers were the same as described above, but in underwater or dry ice environment (~ –80 ^{o}C).

7. Conductivity measurements

Ionic conductivity of the eutectogels was measured by the electrochemical impedance spectroscopy (EIS) method. Impedance data were obtained using a Solartron Analytical Modulab XM CHAS 08 electrochemical workstation in the frequency range of 0.001 Hz to 100 kHz under a variety of temperatures of 60, 40, 25, 0, –20 and –30 ℃. The eutectogel was sandwiched between two stainless steel discs for the measurement. The temperatures were controlled *via* a freezer or oil bath. The ionic conductivity of eutectogels was calculated according to the following equation.

$$\sigma = LR/A$$

where L is the thickness of the eutectogel, R is the impendence value and A is the contact area of the eutectogels.

8. Fabrication of the electrochromic device

The hybrid BGA-12/PHEAA/EV/dmFc eutectogel was *in situ* sandwiched between two ITO-PET substrates to form an electrochromic device. The fabrication of the ECDs was similar as the preparation of the adhesion layers as described above (see Figure 6c in the main text). Briefly, 40.0 mg of BGA-12 (0.072 mM), 1000.0 mg of HEAA (8.7 mM), 46 μL of MBA aqueous (10 mg mL, 0.46 mg, 0.003 mM), 44.8 mg of Irgacure 2959 (0.2 mM), 25.0 mg of ethyl viologen (EV, 0.064 mM) and 30.0 mg of 1,1'-dimethylferrocene (dmFc, 0.12 mM) were completely dissolved into 1.0 mL ChCl/EG (1:2) DES solvent upon heating. The obtained homogenous solution was then cooled to room temperature for BGA-12 gelation. The as-prepared eutectogel samples were sandwiched between two ITO-PET substrates. After *in situ* photopolymerization under the irradiation of a UV lamp (365 nm, 0.4 W cm^{-2}) for ~5 s, resulting in hybrid BGA-12/PHEAA/EV/dmFc SP-DN eutectogels, a completely bubble-free device with uniform SP-DN eutectogel electrolyte film were obtained. The inter-electrode distance was controlled with one layer of double-side tape to obtain the ECD device with a uniform thickness. The effective areas of the ECDs were maintained to be $2.0 \times 2.0 = 4.0$ cm^2.

9. Computational methods

Conformational search was carried out for BGA-12 molecules and representative PHEAA (10 units) segments, and the most stable isomer were selected to construct the supramolecular helical nanowire and the supramolecular-polymer double network. Geometry optimization and frequency analysis of all the species were performed using the semi-empirical PM7 method, which includes dispersion and hydrogen-bond terms in the parametrization step and have been widely used to simulate the formation of noncovalent complexes.[3,4] The single point energies were then calculated using B3LYP functional and 6-311+G(d,p) basis set on the optimized geometries. Grimme's DFT-D3(BJ) dispersion corrections were also carried out in the single-point calculations.[5] All calculations were performed with Gaussian 09.[6] Computed structures were illustrated using CYLView.[7]

Section S2 Synthesis and characterization of bisgluconamide (BGA-n) derivatives

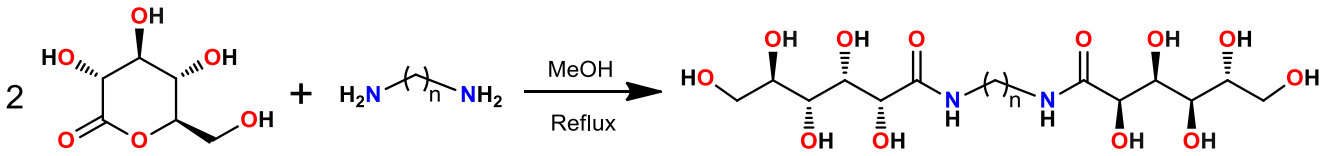

n = 6, 10 and 12

Scheme S1. Synthetic route of bisgluconamide (BGA-n) derivatives.

Synthesis of 1,12-digluconaminododecane (BGA-12).

D-(+)-Gluconic acid δ-lactone (7.1 g, 0.04 mol) were dissolved in 200 mL methanol, followed by stirring for 1 h at 70 ^{o}C under reflux. Afterwards, 1,12-Diaminododecane (8.0 g, 0.04 mol) was added and the reaction mixture was stirred for another 2 h at 70 ℃ under reflux. The mixture was filtered while hot. The residue was washed repeatedly with cold methanol and ether successively, and dried in a vacuum oven resulting in BGA-12 as white solid.

Yield: 6.9 g (~62%). mp: 193.1–194.8 ℃. ^{1}H NMR (500 MHz, DMSO-d_6, 25 °C): δ7.59–7.61 (2H, NH), 5.34–5.36 (2H, OH), 4.54–4.32 (8H, OH), 3.96 (2H, CH), 3.89 (2H, CH), 3.66 (2H, CH), 3.46 (4H, CH_2), 3.36–3.37 (2H, CH), 3.03–3.10 (4H, CH_2), 1.40, (4H, CH_2) 1.24 (16H, CH_2); ^{13}C NMR (150 MHz, DMSO-d6, 25 °C): δ172.69 (2C, C=O), 74.10, 72.87, 71.95, 70.57 (8C, CH), 63.84 (2C, CH_2OH), 38.72, 29.64, 29.54, 29.52, 29.30, 26.85 (12C, CH_2); HR-MS (ESI): m/z calcd. for $C_{24}H_{48}N_2O_{12}H^+$ [M + H]$^+$ 557.32; Anal. calcd. for $C_{24}H_{48}N_2O_{12}$: C, 51.78, H, 8.69, N, 5.03; Found: C, 51.73, H, 8.82, N, 4.84.

Synthesis of 1,10-digluconaminodecane (BGA-10).

BGA-10 was synthesized following the same protocol as BGA-12.

Yield: 6.5 g (~61%). mp: 192.1–193.6 ℃. ^{1}H NMR (500 MHz, DMSO-d_6, 25 °C): δ7.60–7.61 (2H, NH), 5.36 (2H, OH), 4.54–4.34 (8H, OH), 3.96 (2H, CH), 3.89 (2H, CH), 3.56-3.58 (2H, CH), 3.46 (4H, CH_2), 3.37 (2H, CH), 3.03–3.09 (4H, CH_2), 1.40 (4H, CH_2), 1.24 (12H, CH_2); ^{13}C NMR (150 MHz, DMSO-d6, 25 °C): δ 177.44 (2C, C=O), 78.85, 77.62, 76.70, 75.32 (8C, CH), 68.59 (2C, CH_2OH),

43.46, 34.39, 34.23, 34.04, 31.60 (10C, CH_2); HRMS (ESI): m/z calcd for $C_{22}H_{44}N_2O_{12}H^+$ $[M + H]^+$ 529.29; Anal. calcd. for $C_{22}H_{44}N_2O_{12}$: C, 49.99, H, 8.39, N, 5.30; Found: C, 49.74, H, 8.48, N, 5.11.

Synthesis of 1,6-digluconamidohexane (BGA-6).

BGA-6 was synthesized following the same procedure as BGA-12.

Yield: 6.2g (~66%). mp: 183.3–184.1 ℃. ^{1}H NMR (500 MHz, DMSO-d_6, 25 ℃):δ7.59–7.61 (2H, NH), 5.36 (2H, OH), 4.32–4.54 (8H, OH), 3.96–3.98 (2H, CH), 3.88–3.90 (2H, CH), 3.56–3.59 (2H, CH), 3.44–3.49 (4H, CH_2), 3.36–3.38 (2H, CH), 3.02–3.11 (4H, CH_2), 1.39–1.41 (4H, CH_2), 1.24 (4H, CH_2); ^{13}C NMR (150 MHz, DMSO-d6, 25 ℃): δ172.73 (2C, C=O), 74.11, 72.87, 71.93, 70.56 (8C, CH), 63.82 (2C, CH_2OH), 38.66, 29.58, 26.54 (6C, CH_2); HRMS (ESI): m/z calcd for $C_{18}H_{36}N_2O_{12}Na^+$ $[M + Na]^+$ 495.23; Anal. calcd. for $C_{18}H_{36}N_2O_{12}$: C, 45.76, H, 7.68, N, 5.93; Found: C, 45.75, H, 7.79, N, 5.63.

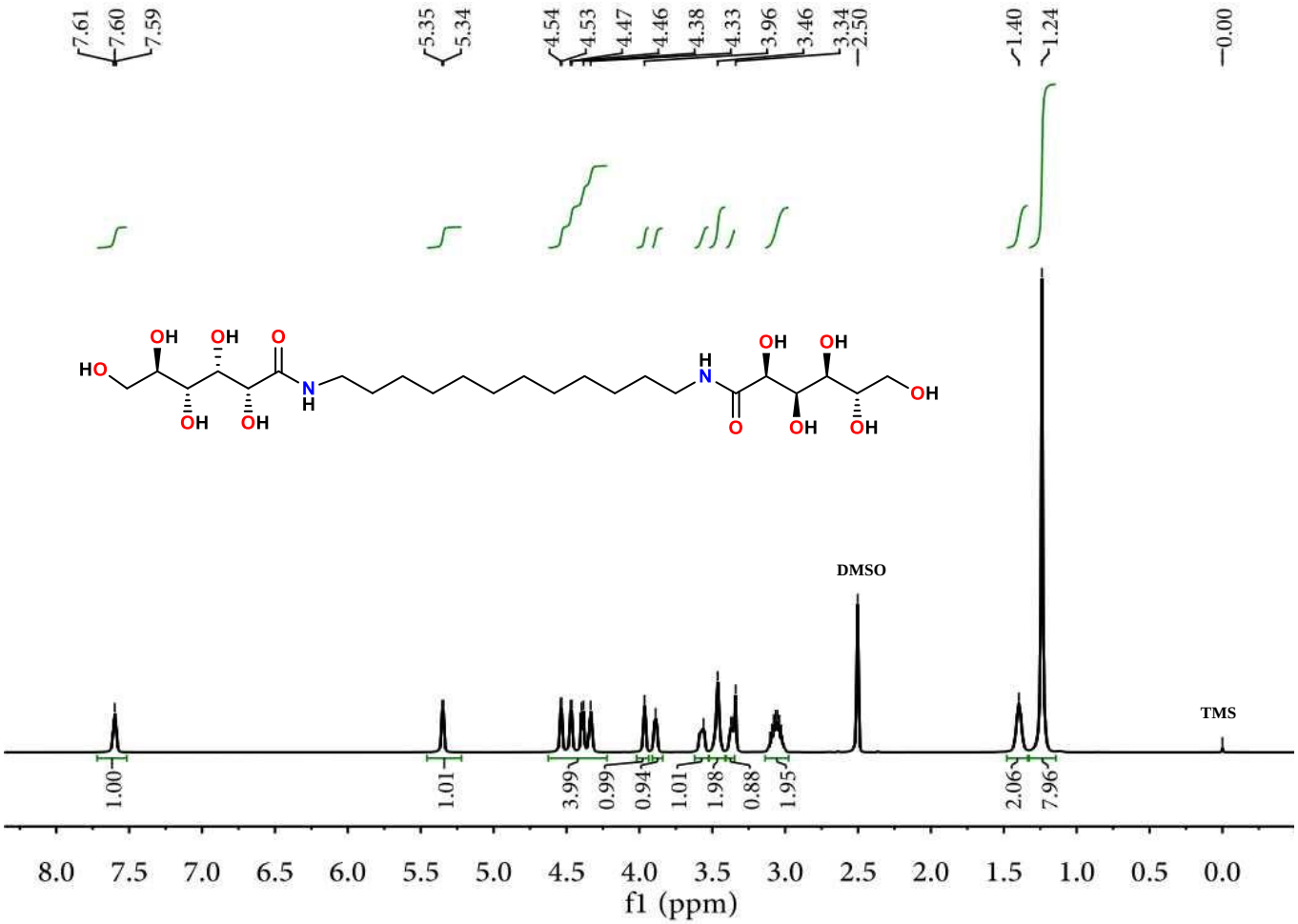

Figure S4. ^{1}H NMR spectrum of BGA-12 (500 MHz, DMSO-d_6, 25 ^{o}C).

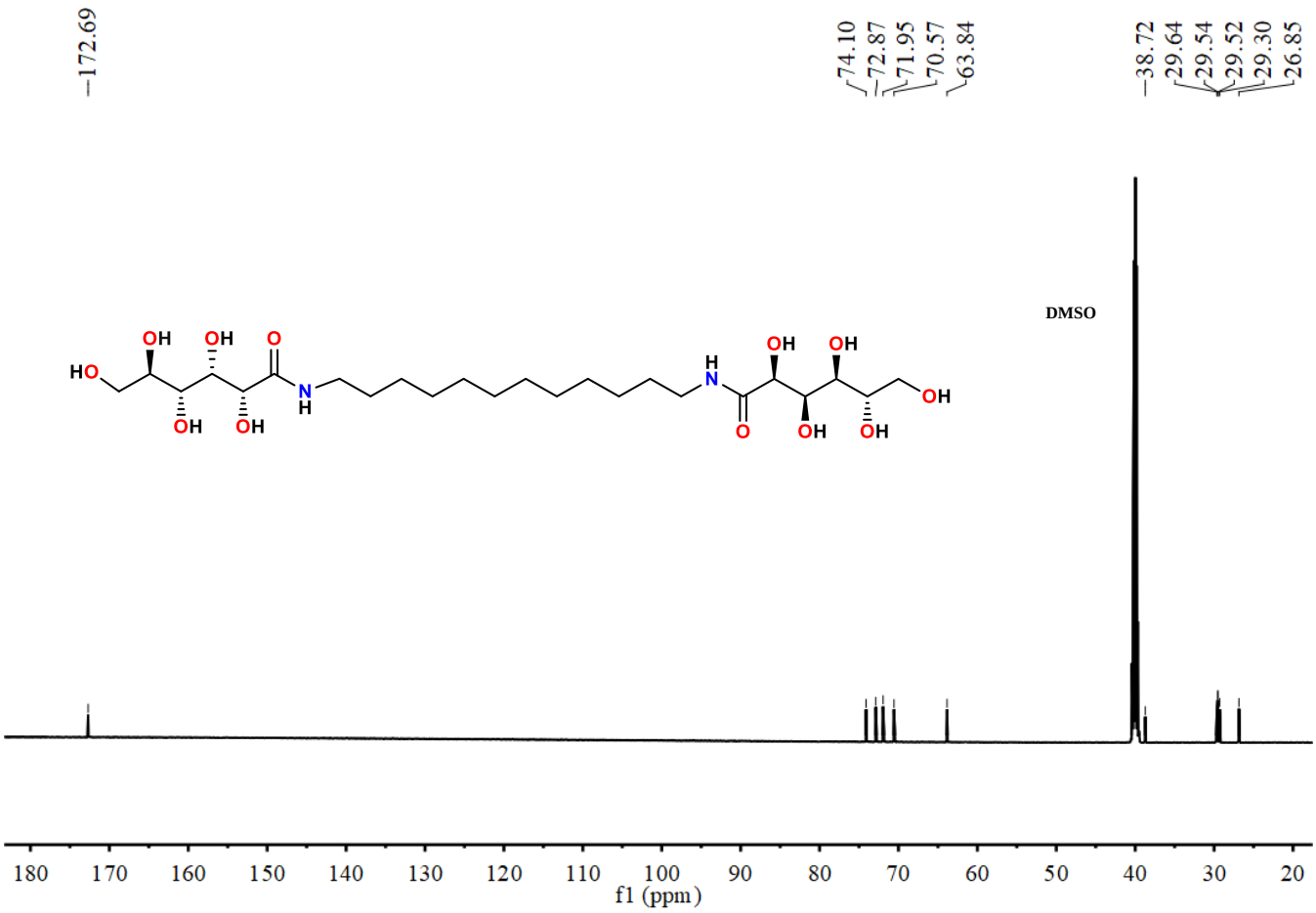

Figure S5. ^{13}C NMR spectrum of BGA-12 (150 MHz, DMSO-d_6, 25 ^{o}C).

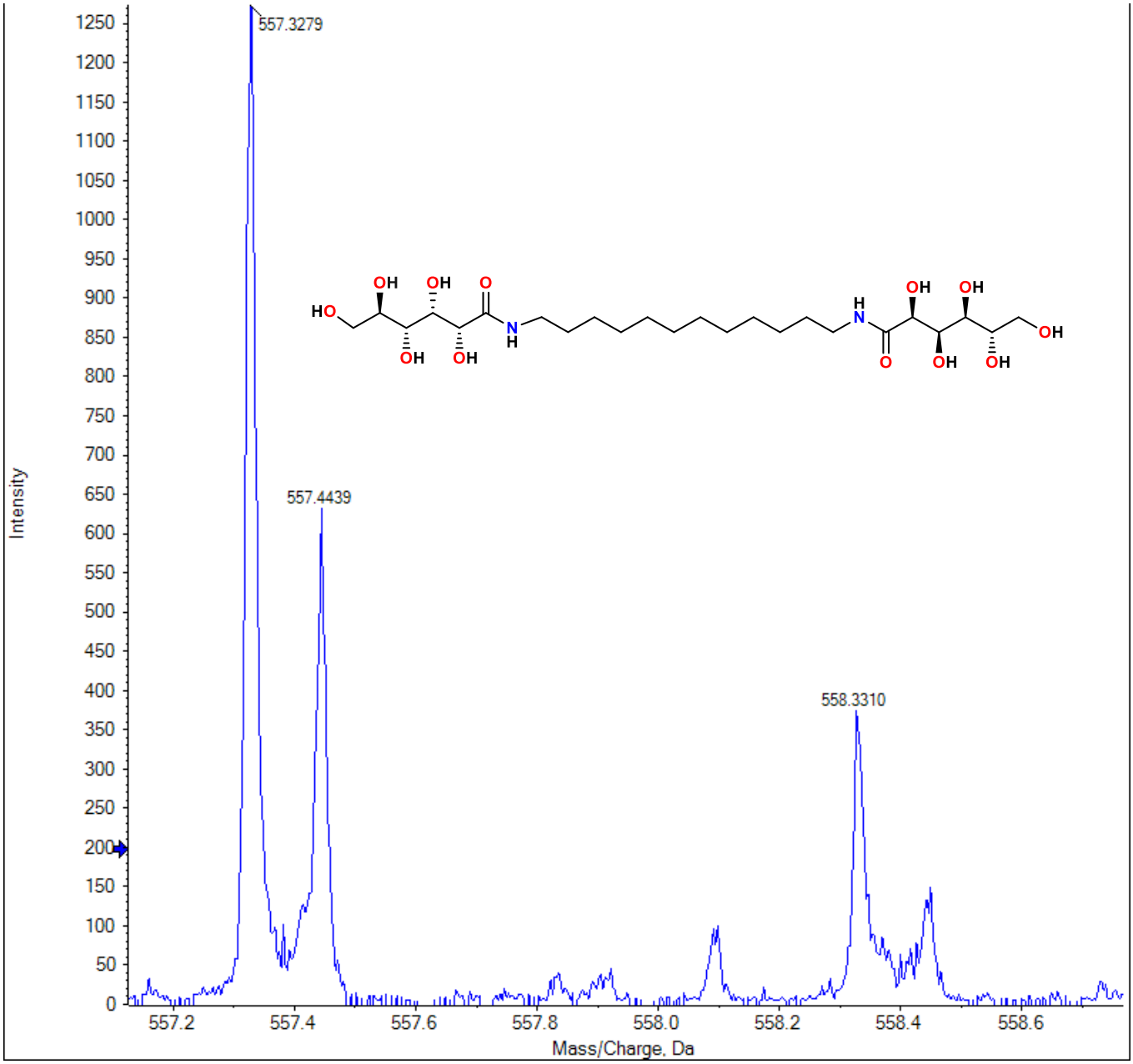

Figure S6. HR-MS spectrum of BGA-12 ($M + H^+$).

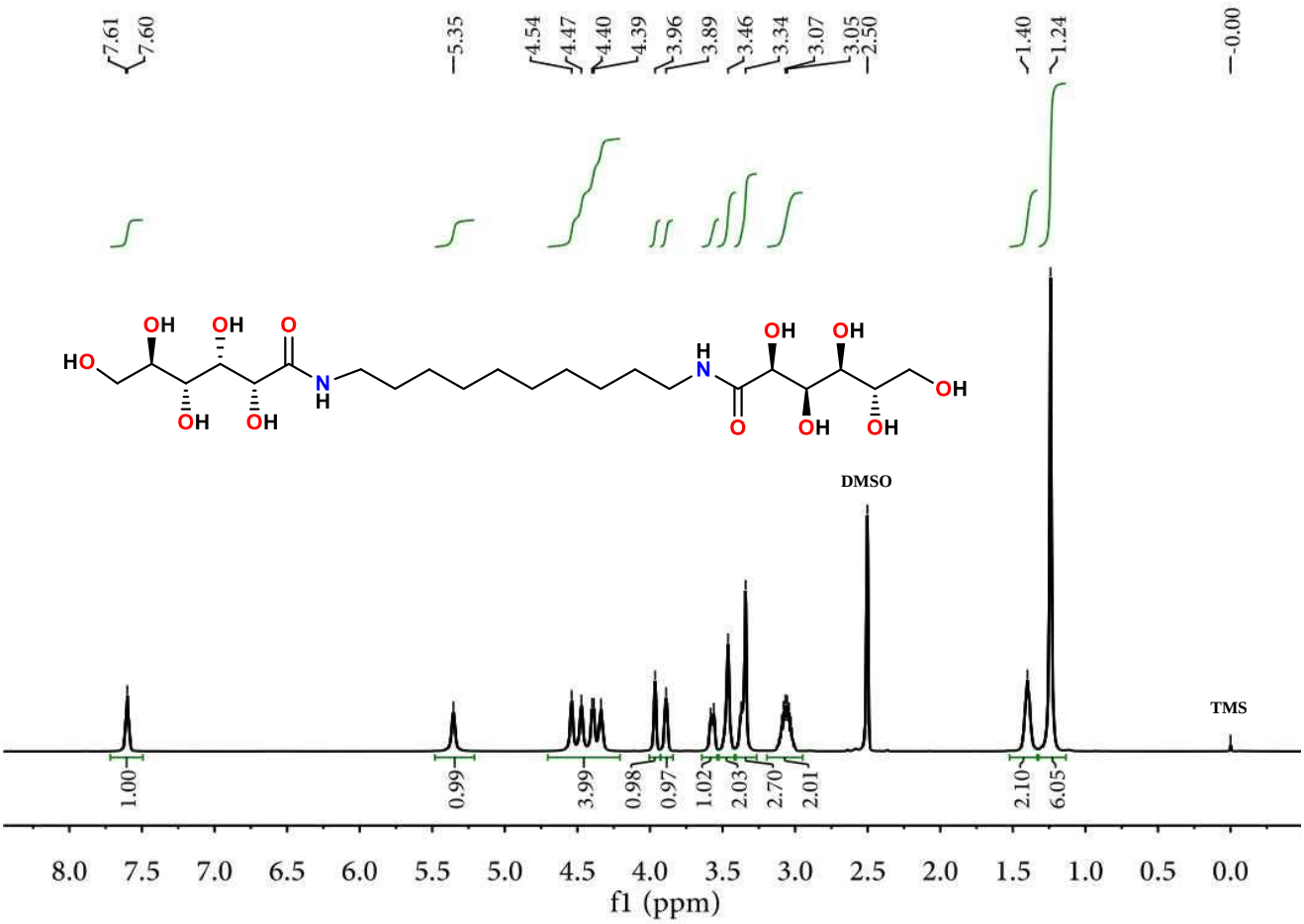

Figure S7. ^{1}H NMR spectrum of BGA-10 (500M, DMSO-d_6, 25 ^{o}C).

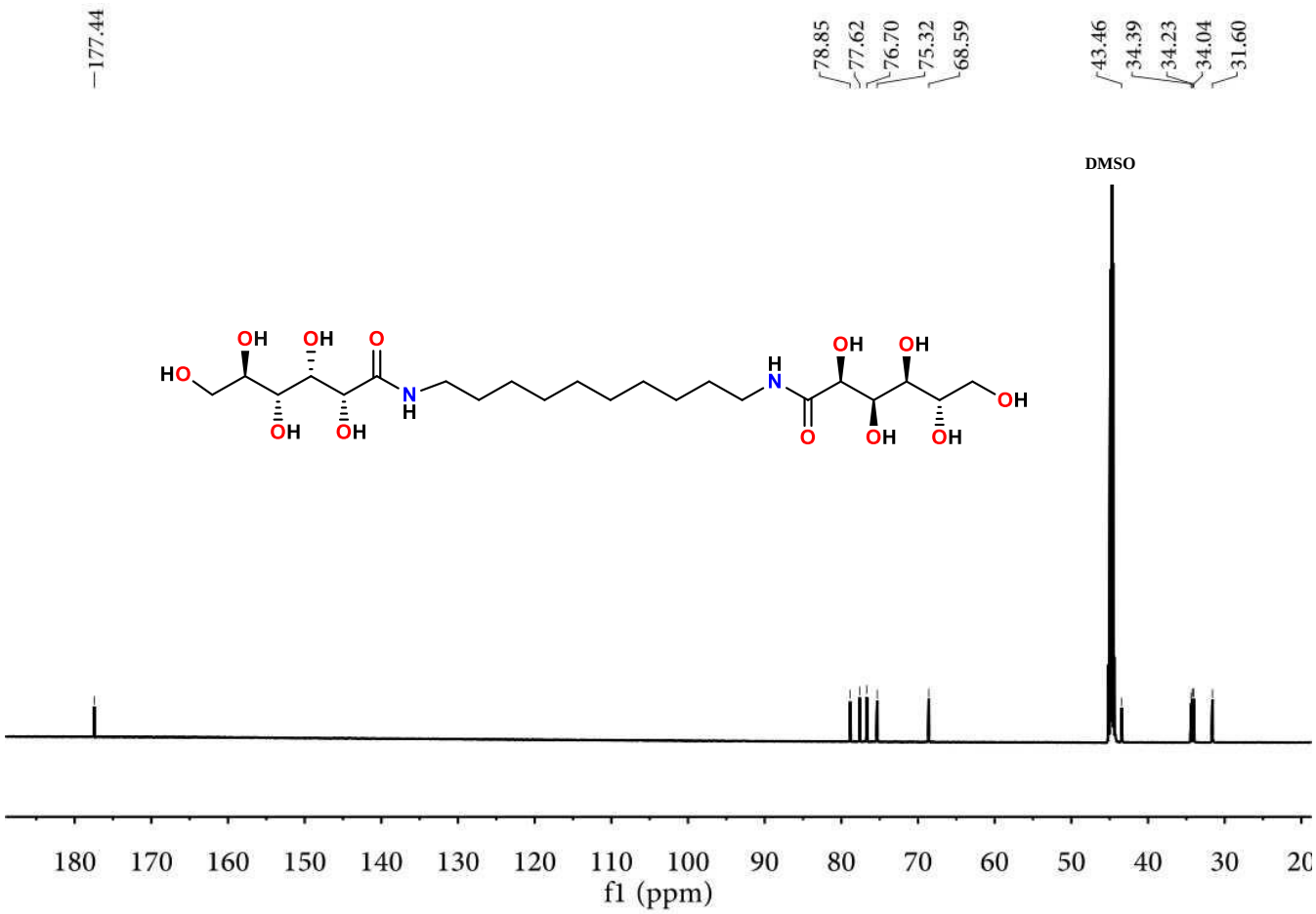

Figure S8. ^{13}C NMR spectrum of BGA-10 (150 MHz, DMSO-d_6, 25 ^{o}C).

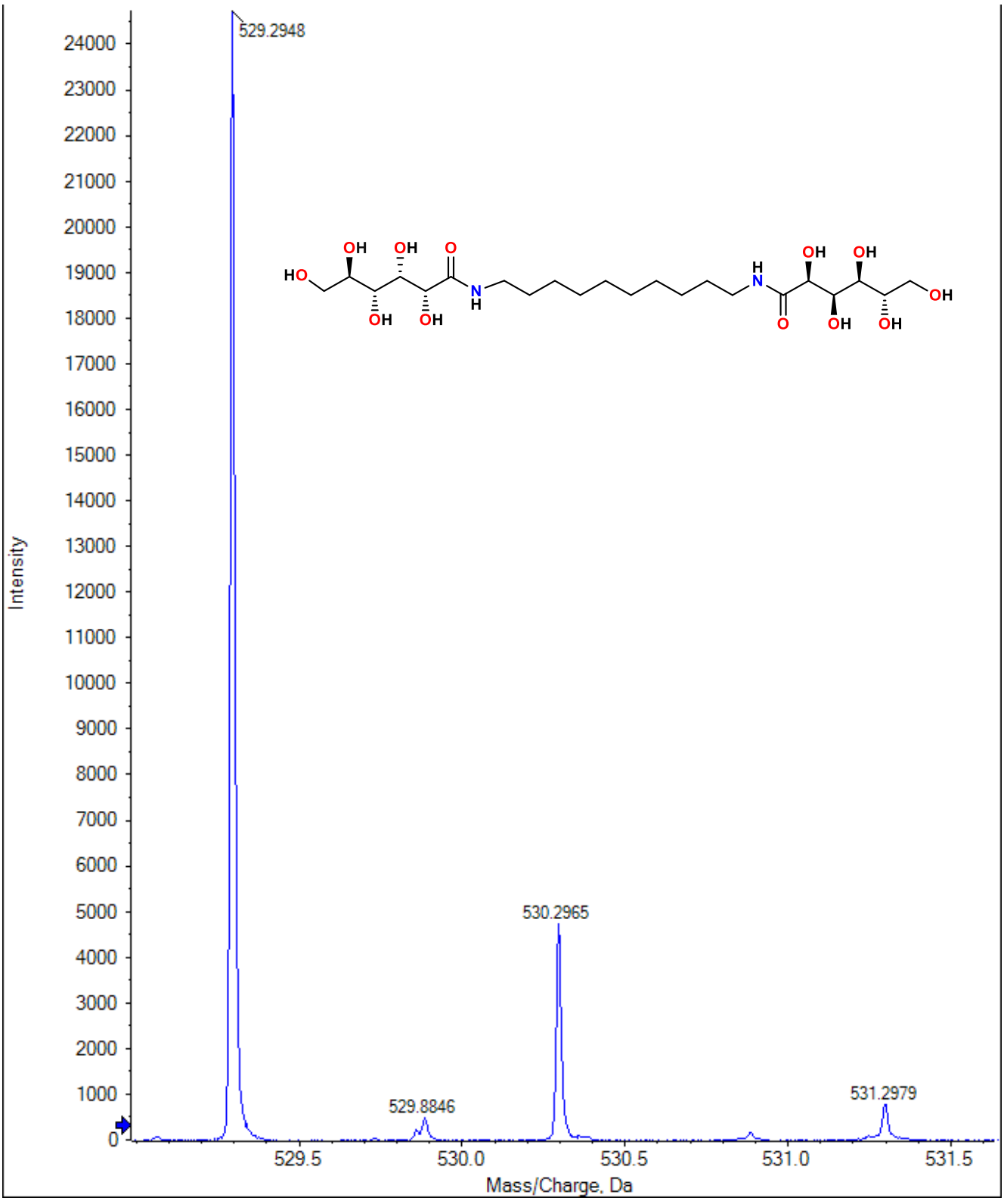

Figure S9. HR-MS spectrum of BGA-10 ($M + H^+$).

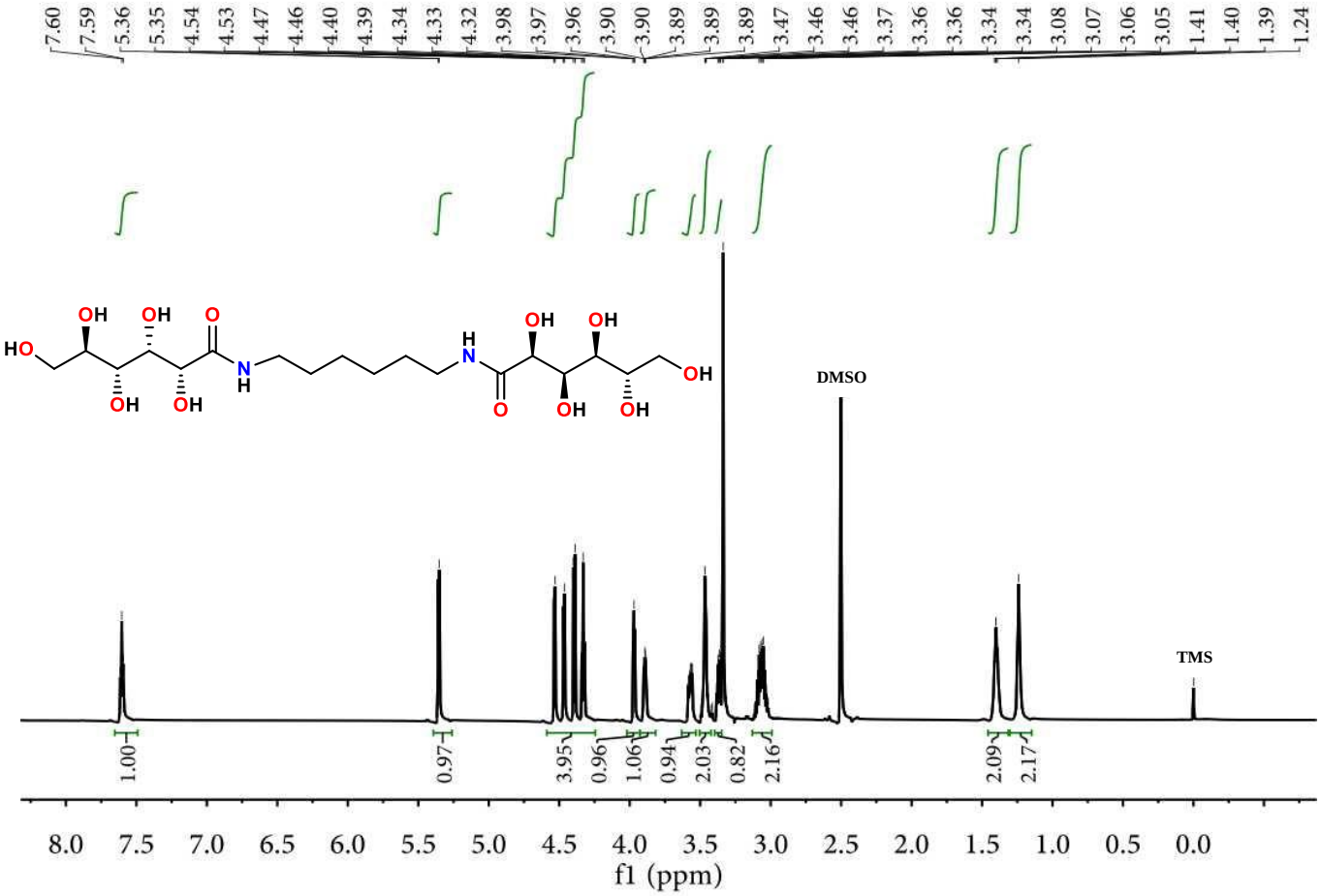

Figure S10. ^{1}H NMR spectrum of BGA-6 (500 M, DMSO-d_6, 25 ^{o}C).

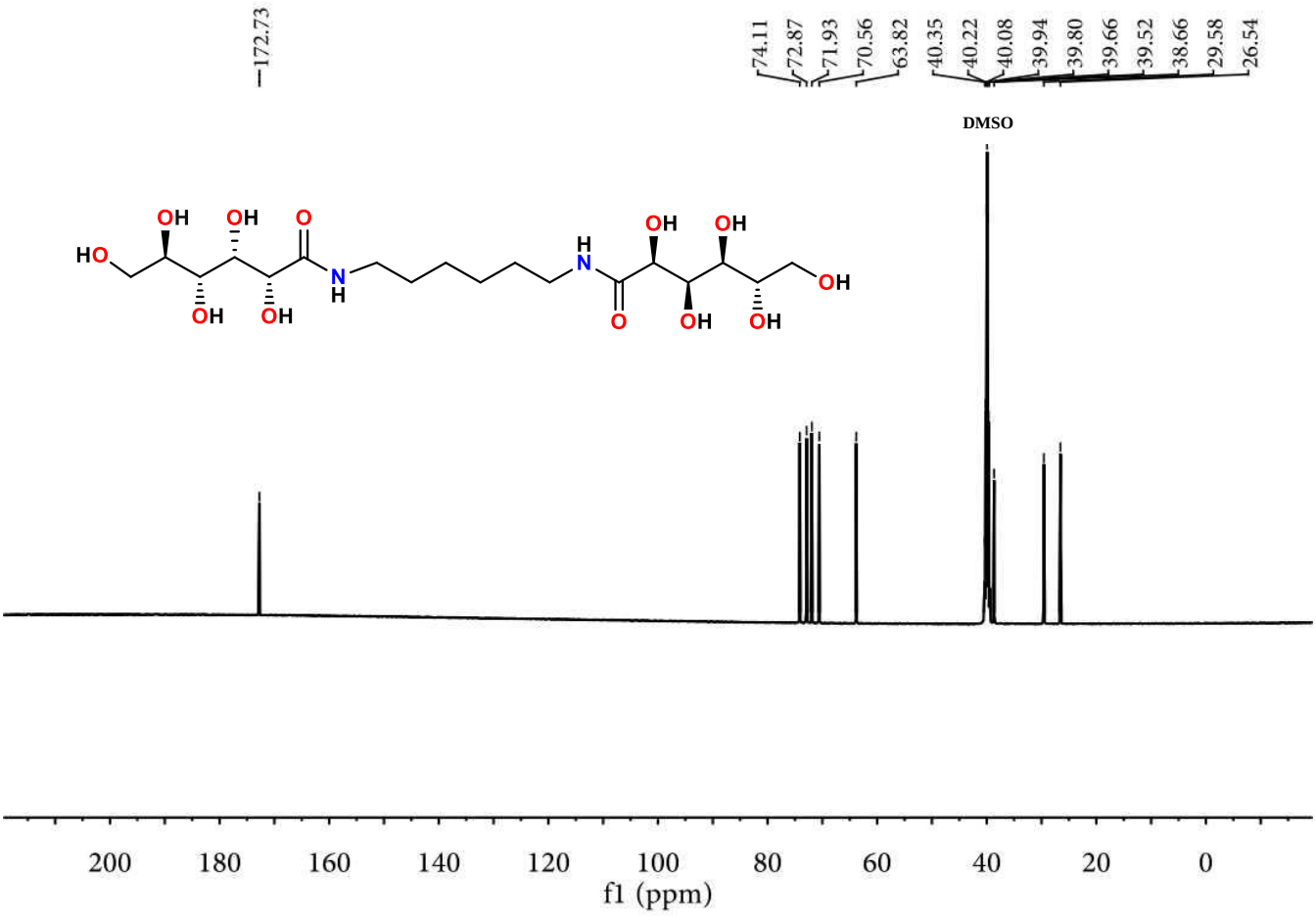

Figure S11. ^{13}C NMR spectrum of BGA-6 (150 MHz, DMSO-d_6, 25 ^{o}C).

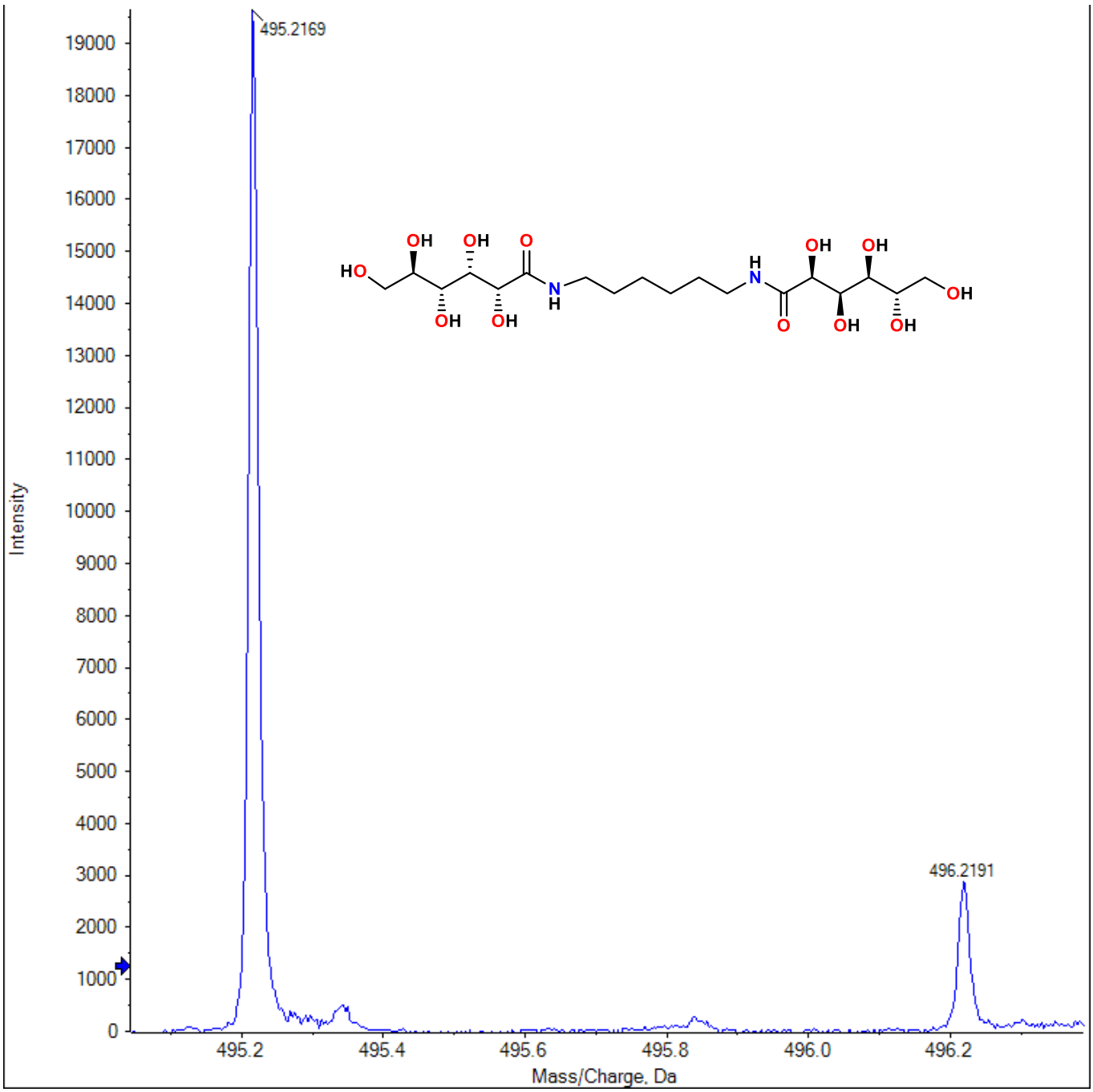

Figure S12. HR-MS spectrum of BGA-6 ($M + Na^+$).

Section S3 Gelation properties of BGA-n (n = 6, 10 and 12) single-network (SN) eutectogels

Table S1. Gelation behaviors of BGA-n, including apearances, gel-to-sol phase transformatin temperatures (T_{gels}, ℃) of eutectogels with 6% w/v gelator, and critical gelator concentrations (CGCs, w/v%) in different DESs.

DESs	Gelator		
	BGA-6	**BGA-10**	**BGA-12**
choline chloride/ glycerol (1:2)	Vs	OG 82.5−84.1 ℃ 3.8%	OG 116.0−119.2 ℃ 3.5%
choline chloride/ ethylene glycerol (1:2)	S	OG 72.2−74.3 ℃ 4.2%	OG 102.6−105.9 ℃ 1.4%
choline chloride/ propylene glycol (1:2)	S	OG 65.6−67.2 ℃ 4.2%	OG 91.5−93.6 ℃ 2.1%
choline chloride/ propane-1,3-Diol (1:2)	S	Vs	OG 115.5−117.0 ℃ 1.6%

OG = opaque gel; Vs = viscous liquid; S = solution.

Gelation behaviors of BGA-n in various DESs was evaluated by a inverted tube method. T_{gels} were determined at the concentration of 6% (w/v) BGA-n by using the "falling-ball method". CGCs were recoreded as the minium concentration of BGA-n that needed to form a stable eutectogel.

Figure S13. The injectable capacity of the BGA-12 eutectogel. The droplets of soft BGA-12 eutectogel were injected by a syringe with increasing sizes and heights. Red dyes of rhodamine B were added to visually observe the BGA-12 eutectogel.

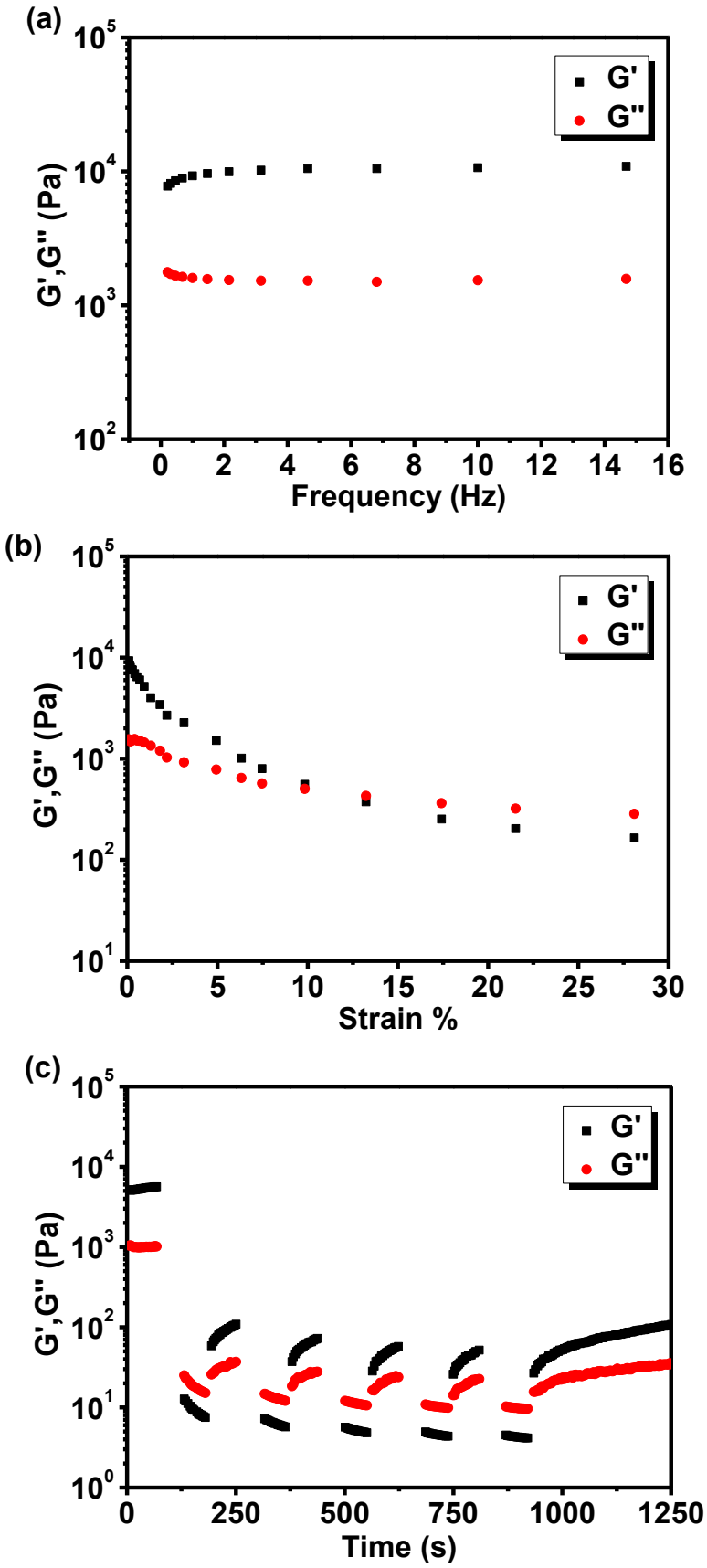

Figure S14. (a) Dynamic frequency sweep, (b) oscillatory strain sweep and (c) step-strain sweep of 6% w/v BGA-10 eutectogel.

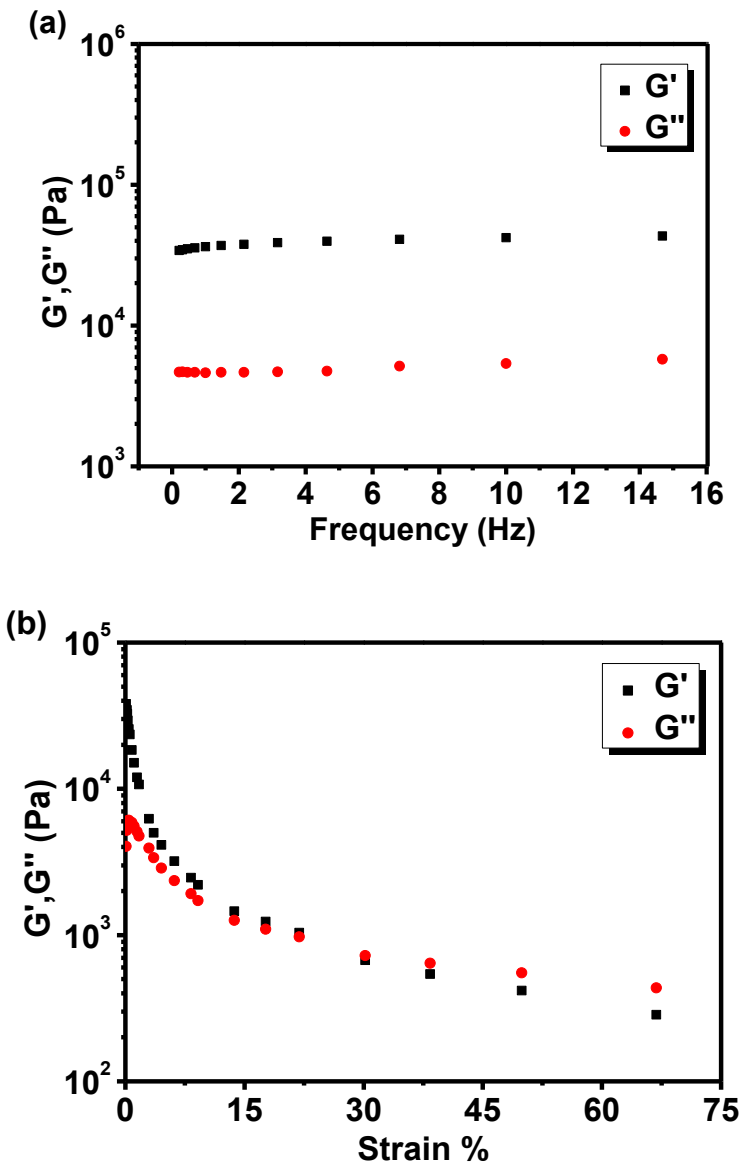

Figure S15. (a) Dynamic frequency sweeps and (b) oscillatory strain sweep of 6% w/v BGA-12 eutectogel. Rheological test further demonstrated the particular mechanical properties of these eutectogels. As shown in Figures S14 and S15, the storage modulus (G') of both BGA-10 and BGA-12 eutectogels is consistently higher than the loss modulus (G''), which is independent of frequency over the entire investigated range. The G' of BGA-10 eutectogel (ca 1.0×10^4 Pa) was much lower than BGA-12 eutectogel (ca 4.0×10^4 Pa), indicating the softer feature of BGA-10 eutectogel compared to BGA-12 eutectogel. Oscillatory strain sweep suggested that the yield strain of both eutectogels were around 10−15%, indicating that less energy is needed to initiate the flow. Step-strain measurement (see Figure 1b in the main text and Figure S14c) by applying an alternative large strain of 100% to destroy the gel and a low strain of 0.1% for gel recovery, further confirmed that both gels exhibited favorable thixotropic properties.

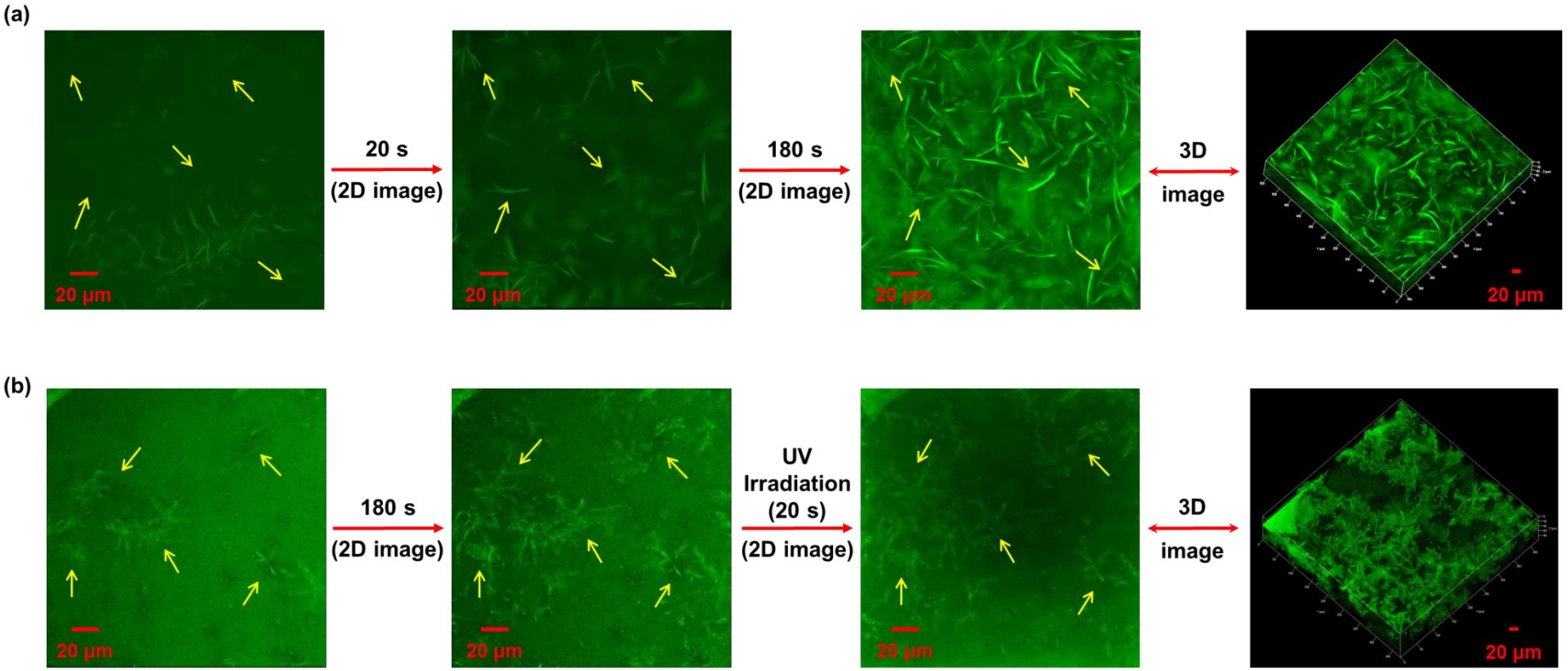

Figure S16. Structure evolution of lamellar supramolecular eutectogel and fibrillar SP-DN eutectogel evaluated by real-time *in situ* imaging. Time-lapse CLSM images of (a) the BGA-12 and (b) the BGA-12/PHEAA SP-DN eutectogel under different time intervals, as well as their final 3D CLSM images. The samples were being observed immediately upon the precursor hot solution was dropped onto the object slide. Both eutectogels were labeled with fluorescein isothiocyanate (FITC), green fluorescence probe.

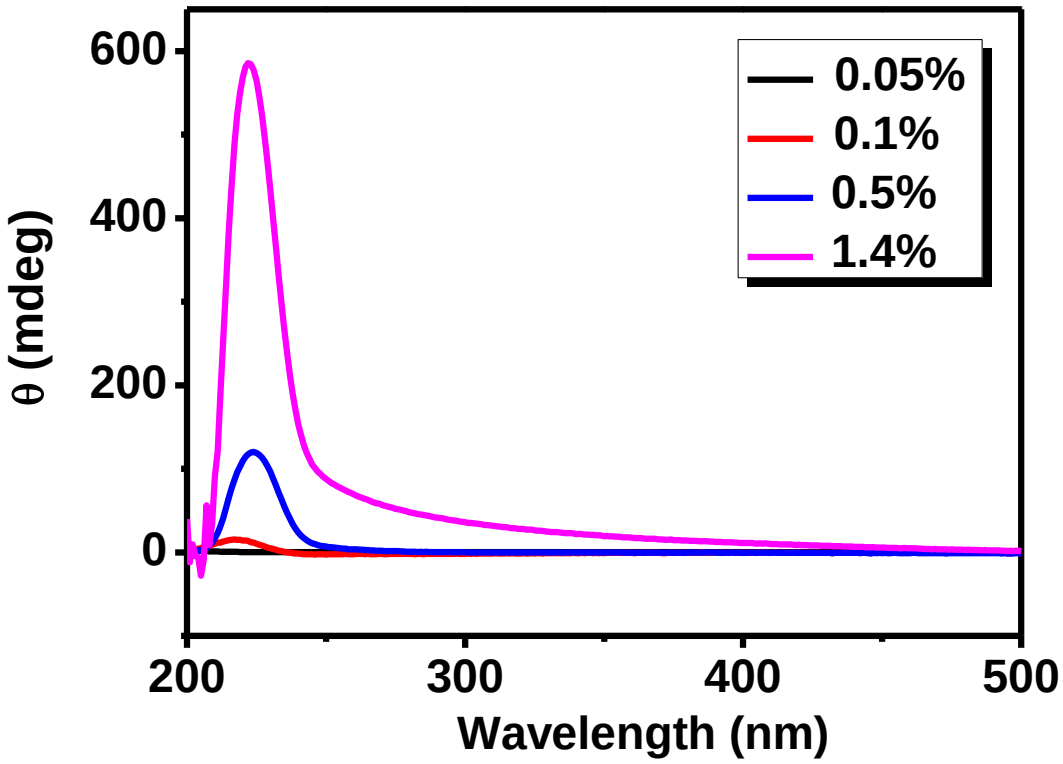

Figure S17. Supramolecular chirality of the BGA-12 eutectogel. Variable-concentration CD spectra of the BGA-12 eutectogel in choline chloride/ethylene glycerol (1:2). Variable-concentration CD spectra displayed that, with increasing concentration of the BGA-12 in choline chloride/ethylene glycerol (1:2), a positive CD signal at round 222 nm gradually appeared and intensified along with the aggregation of BGA-12 molecules. Variable-temperature CD spectra (see Figure 1d in the main text) of 0.5% BGA-12 eutectogel further confirm that the CD signal gradually decreased with increasing temperature, which can be attributed to the disassociation of BGA-12 supramolecules. The results suggested the formation of right-handed stacking of BGA-12 molecules within the eutectogel.

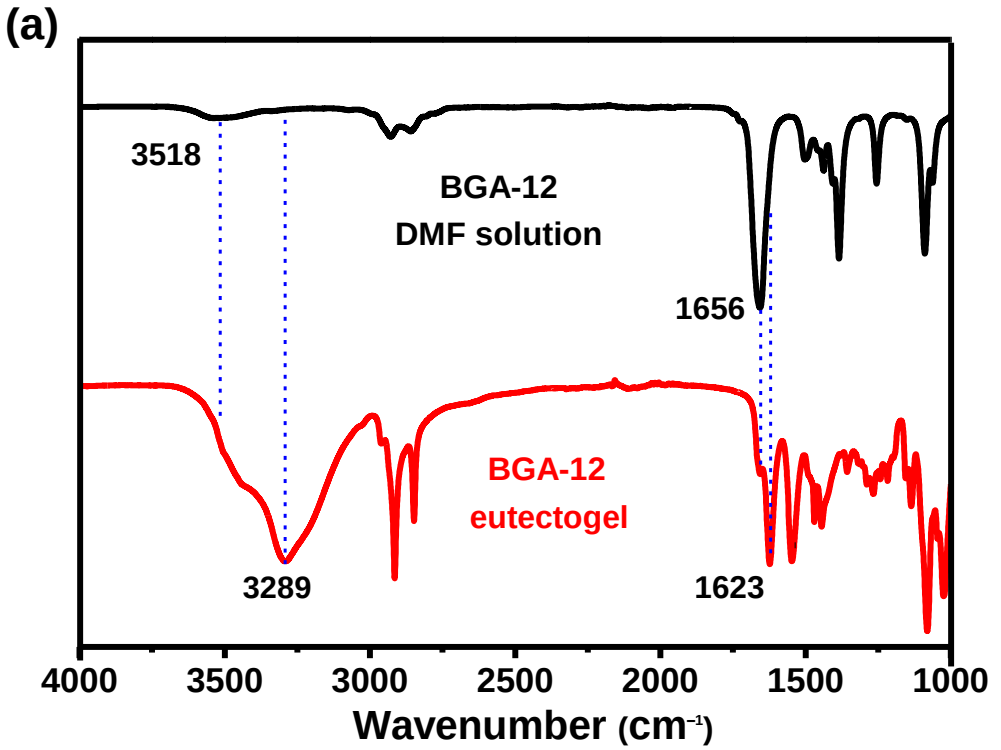
(a)
3518
BGA-12
DMF solution
1656
BGA-12
eutectogel
3289
1623
4000
3500
3000
2500
2000
1500
1000
Wavenumber (cm⁻¹)

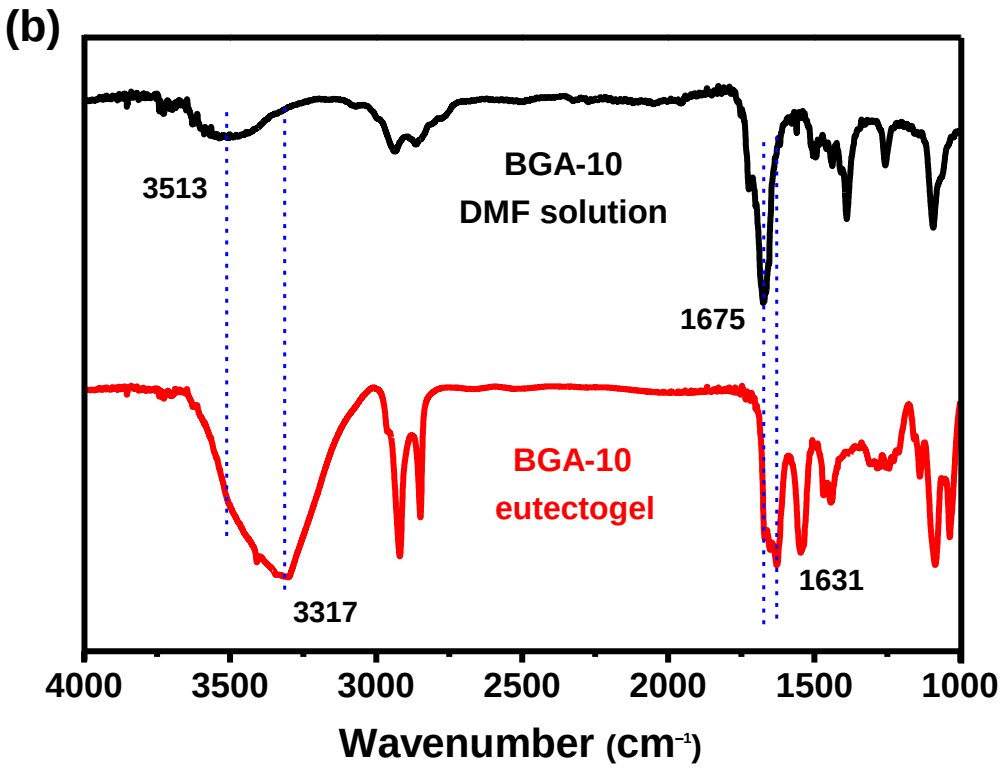
(b)
3513
BGA-10
DMF solution
1675
BGA-10
eutectogel
3317
1631
4000
3500
3000
2500
2000
1500
1000
Wavenumber (cm⁻¹)

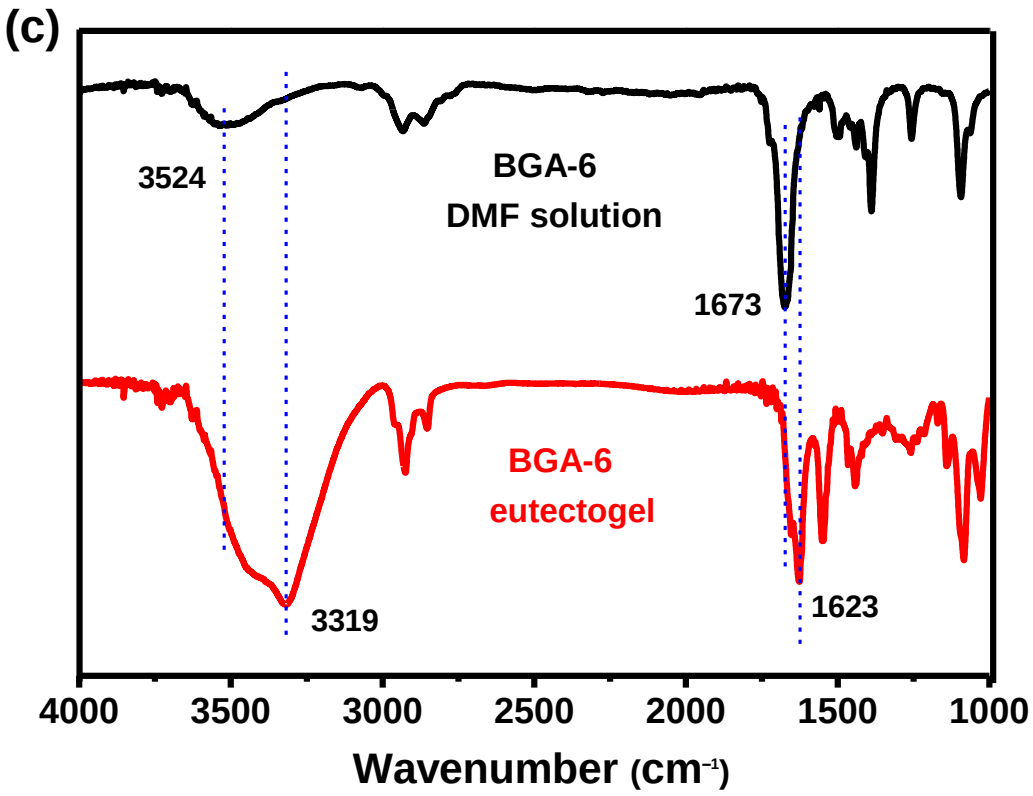

Figure S18. Hydrogen-bonding interaction between BGA-n molecules for gelation. FTIR spectra of the BGA-n in DMF solutions and the BGA-n eutectogels in choline chloride/ethylene glycerol (1:2): (a) for BGA-12, (b) for BGA-10, and (c) for BGA-6.

The FTIR of the BGA-12 in DMF solution displays a broad band appearing at 3518 cm^{-1} and a sharp band at 1656 cm^{-1}, assigning to the stretching vibrations of OH (NH) and C=O, respectively. However, in the BGA-12 eutectogel, these bands shift to 3289 and 1623 cm^{-1}, respectively. Similarly, the stretching vibrations of OH (NH) and C=O in the FTIR spectra of BGA-6 and BGA-10 eutectogels also shift towards lower wavenumbers, as shown in Figures S18b and c. These results provide direct evidence for the formation of hydrogen-bonding interactions between BGA-n molecules for gelation.

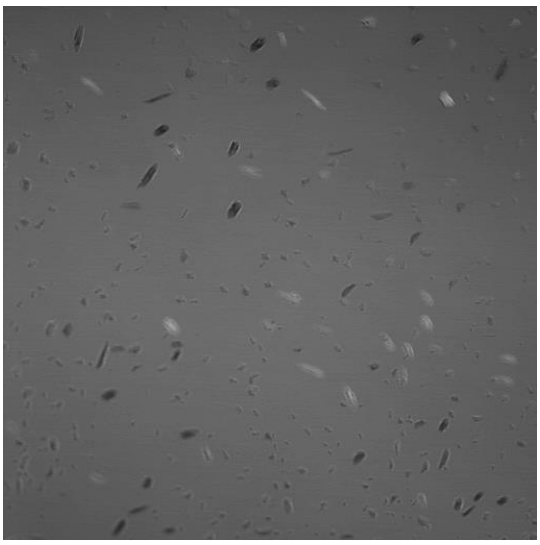

Figure S19. Microstructure of the PHEAA single-netwrok eutectogel. Bright-field CLSM image of the PHEAA eutectogel, showing aggregated nanoclusters which could not be labeled by commercially available fluorescence probes including FITC.

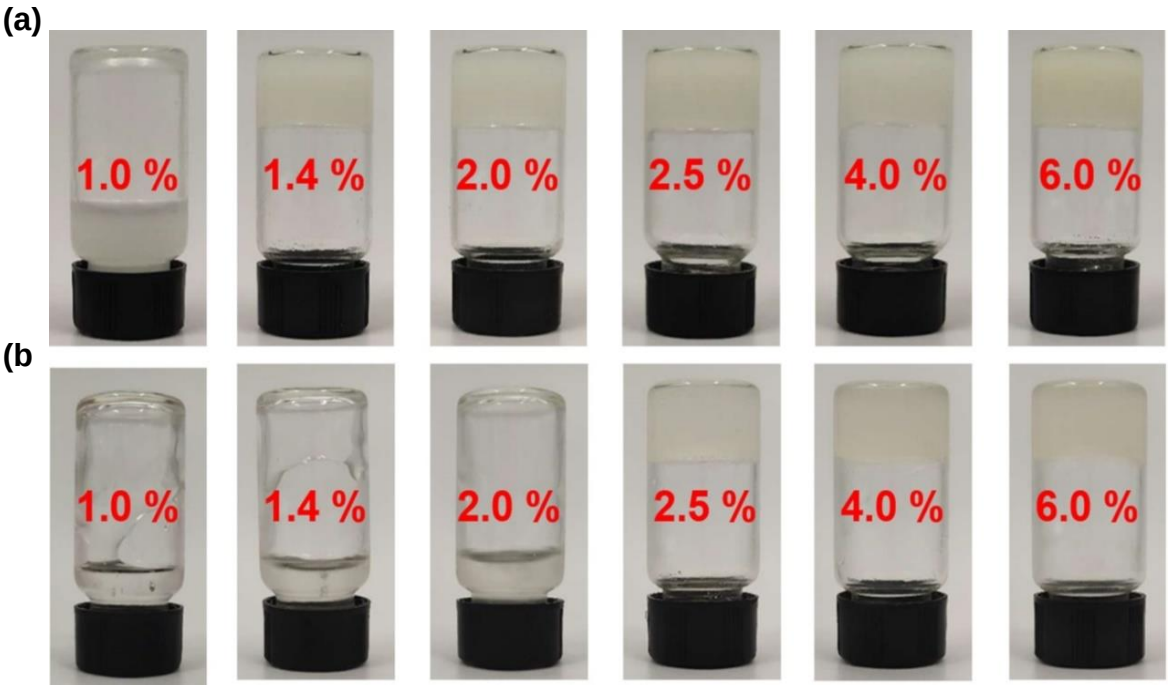

Figure S20. Effects of polymer species on the gelation behaviors of BGA-12 molecules. Appearances of BGA-12 molecules in ChCl/EG in the (a) absence and (b) presence of polymer precursors at different concentrations, highlighting higher critical gelator concentration (2.5% w/v) of BGA-12 molecules in the presence of polymer precursors compared to that (1.4% w/v) in the pure DESs.

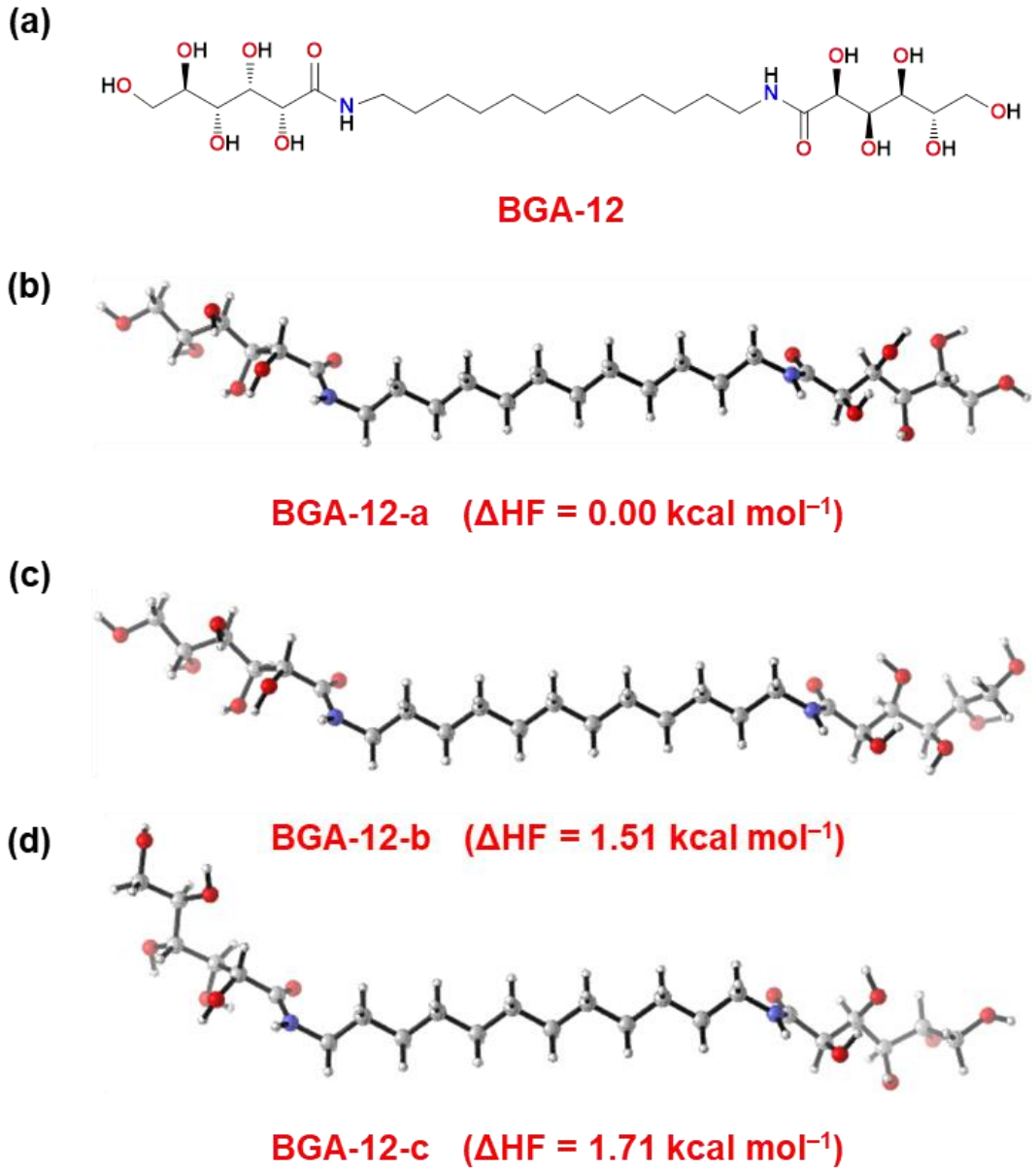

Figure S21. Computer simulation of BGA-12 molecules. Chemical structure of (a) BGA-12 and (c-d) PM7 optimized geometries and calculated relative heats of formation (ΔHF) of the three most stable BGA-12 isomers. BGA-12-a isomer with the lowest energy was selected to construct the supramolecular helical nanowire in the subsequent calculations.

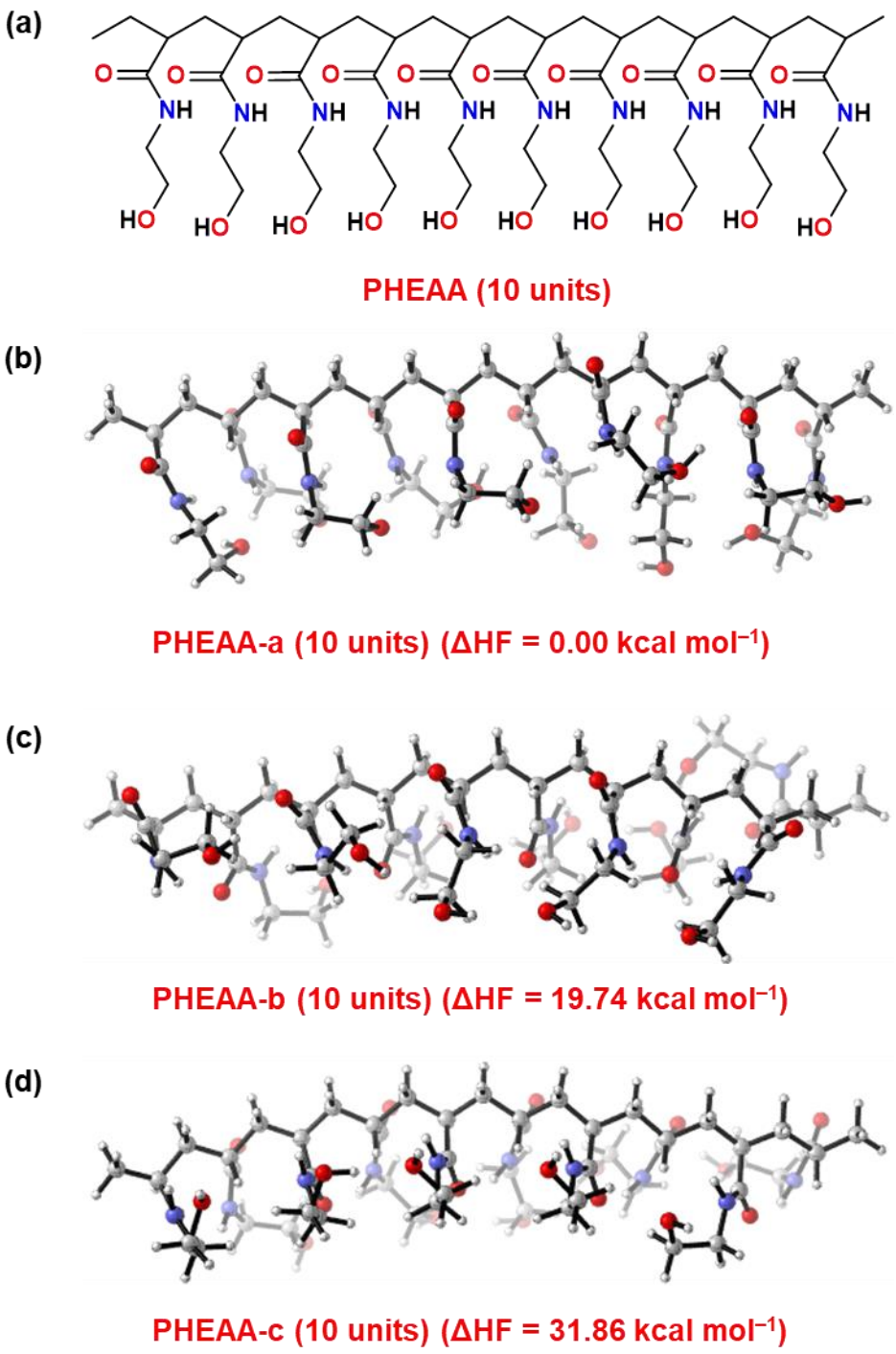

Figure S22. Computer simulation of PHEAA segments. Chemical structure of (a) PHEAA segments (10 units) and (c-d) PM7 optimized geometries and calculated relative heats of formation (ΔHF) of the three most stable PHEAA (10 units) isomers. PHEAA-a isomer with the lowest energy was selected to construct the supramolecular-polymer double network in the subsequent calculations.

Table S2. The calculated energies of the species discussed in the main text based on B3LYP-D3(BJ)/6-31+G(d,p)//PM7.

Species	Energy (Hartree)
BGA-12	–1956.3921471
$(BGA\text{-}12)_6$	–11738.699639
PHEAA (10 units)	–4053.7545242
$(BGA\text{-}12)_6$/PHEAA	–15792.5301758

Table S3. The calculated interaction energies based on B3LYP-D3(BJ)/6-311+G(d,p)//PM7[a].

Reactions	E_{inter} (kcal mol^{-1})
6 **BGA–**12 → **$(BGA–12)_6$**	–217.59
$(BGA–12)_6$ + **PHEAA (**10 **units)** → **$(BGA–12)_6$/PHEAA**	–47.70

[a] For a given reaction, for example, A + B → complex, the interaction energy is calculated by the following equation: $E_{inter} = E_{complex} – E_A – E_B$.

Section S4 Mechanical performance of the BGA-12/PHEAA supramolecular-polymer double-network (SP-DN) eutectogel

Table S4. Effect of BGA-12 content on the BGA-12/PHEAA SP-DN eutectogel.

	BGA-12 (mg)	HEAA (g)	MBA[a] (μL)	Irgacure 2959 (mg)	Irradiation time (s)	DES (mL)	Tensile fracture stress (MPa)	Tensile fracture strain (mm mm^{-1})	Work of extension at fracture (MJ m^{-3})
(BGA-12)$_x$-HEAA$_y$-MBA$_z$-t	0.0	1.0	46	44.8	60	1.0	0.12	28.7	1.4
(BGA-12)$_x$-HEAA$_y$-MBA$_z$-t	30.0	1.0	46	44.8	60	1.0	0.33	54.0	5.5
(BGA-12)$_x$-HEAA$_y$-MBA$_z$-t	40.0	1.0	46	44.8	60	1.0	0.37	56.5	8.8
(BGA-12)$_x$-HEAA$_y$-MBA$_z$-t	60.0	1.0	46	44.8	60	1.0	0.31	39.5	5.5

The compositions of the SP-DN eutectogels were referred as (BGA-12)$_x$-HEAA$_y$-MBA$_z$-t: where x is the mass of BGA-n (mg), y is the mass of HEAA (mg), z is the volume of MBA solution and t is the irradiation time of the UV lamp.[a] The concentration of MBA solution was 10 mg mL^{-1}.

Table S5. Effect of HEAA content on the BGA-12/PHEAA SP-DN eutectogel.

	BGA-12 (mg)	HEAA (g)	MBA[a] (μL)	Irgacure 2959 (mg)	Irradiation time (s)	DES (mL)	Tensile fracture stress (MPa)	Tensile fracture strain (mm mm^{-1})	Work of extension at fracture (MJ m^{-3})
(BGA-12)$_x$-HEAA$_y$-MBA$_z$-t	40.0	0.5	46	44.8	60	1.0	0.08	39.5	1.4
(BGA-12)$_x$-HEAA$_y$-MBA$_z$-t	40.0	0.8	46	44.8	60	1.0	0.23	49.0	4.0
(BGA-12)$_x$-HEAA$_y$-MBA$_z$-t	40.0	1.0	46	44.8	60	1.0	0.37	56.5	8.8
(BGA-12)$_x$-HEAA$_y$-MBA$_z$-t	40.0	1.5	46	44.8	60	1.0	0.21	27.2	2.7

The compositions of the SP-DN eutectogels were referred as (BGA-12)$_x$-HEAA$_y$-MBA$_z$-t: where x is the mass of BGA-n (mg), y is the mass of HEAA (mg), z is the volume of MBA solution and t is the irradiation time of the UV lamp.[a] The concentration of MBA solution was 10 mg mL^{-1}.

Table S6. Effect of MBA content on the BGA-12/PHEAA SP-DN eutectogel.

	BGA-12 (mg)	HEAA (g)	MBA[a] (μL)	Irgacure 2959 (mg)	Irradiation time (s)	DES (mL)	Tensile fracture stress (MPa)	Tensile fracture strain (mm mm^{-1})	Work of extension at fracture (MJ m^{-3})
(BGA-12)$_x$-HEAA$_y$-MBA$_z$-t	40.0	1.0	12	44.8	60	1.0	0.03	65.2	1.4
(BGA-12)$_x$-HEAA$_y$-MBA$_z$-t	40.0	1.0	23	44.8	60	1.0	0.06	38.8	1.3
(BGA-12)$_x$-HEAA$_y$-MBA$_z$-t	40.0	1.0	46	44.8	60	1.0	0.37	56.4	8.8
(BGA-12)$_x$-HEAA$_y$-MBA$_z$-t	40.0	1.0	69	44.8	60	1.0	0.10	28.4	1.3
(BGA-12)$_x$-HEAA$_y$-MBA$_z$-t	40.0	1.0	92	44.8	60	1.0	0.19	31.5	2.3

The compositions of the SP-DN eutectogels were referred as (BGA-12)$_x$-HEAA$_y$-MBA$_z$-t: where x is the mass of BGA-n (mg), y is the mass of HEAA (mg), z is the volume of MBA solution and t is the irradiation time of the UV lamp.[a] The concentration of MBA solution was 10 mg mL^{-1}.

Table S7. Effect of irradiation time on the BGA-12/PHEAA SP-DN eutectogel.

	BGA-12 (mg)	HEAA (g)	MBA[a] (μL)	Irgacure 2959 (mg)	Irradiation time (s)	DES (mL)	Tensile fracture stress (MPa)	Tensile fracture strain (mm mm^{-1})	Work of extension at fracture (MJ m^{-3})
(BGA-12)$_x$-HEAA$_y$-MBA$_z$-t	40.0	1.0	46	44.8	5	1.0	0.22	37.8	3.5
(BGA-12)$_x$-HEAA$_y$-MBA$_z$-t	40.0	1.0	46	44.8	30	1.0	0.33	41.4	4.9
(BGA-12)$_x$-HEAA$_y$-MBA$_z$-t	40.0	1.0	46	44.8	60	1.0	0.37	56.5	8.8
(BGA-12)$_x$-HEAA$_y$-MBA$_z$-t	40.0	1.0	46	44.8	90	1.0	0.34	61.3	6.6

The compositions of the SP-DN eutectogels were referred as (BGA-12)$_x$-HEAA$_y$-MBA$_z$-t: where x is the mass of BGA-n (mg), y is the mass of HEAA (mg), z is the volume of MBA solution and t is the irradiation time of the UV lamp.[a] The concentration of MBA solution was 10 mg mL^{-1}.

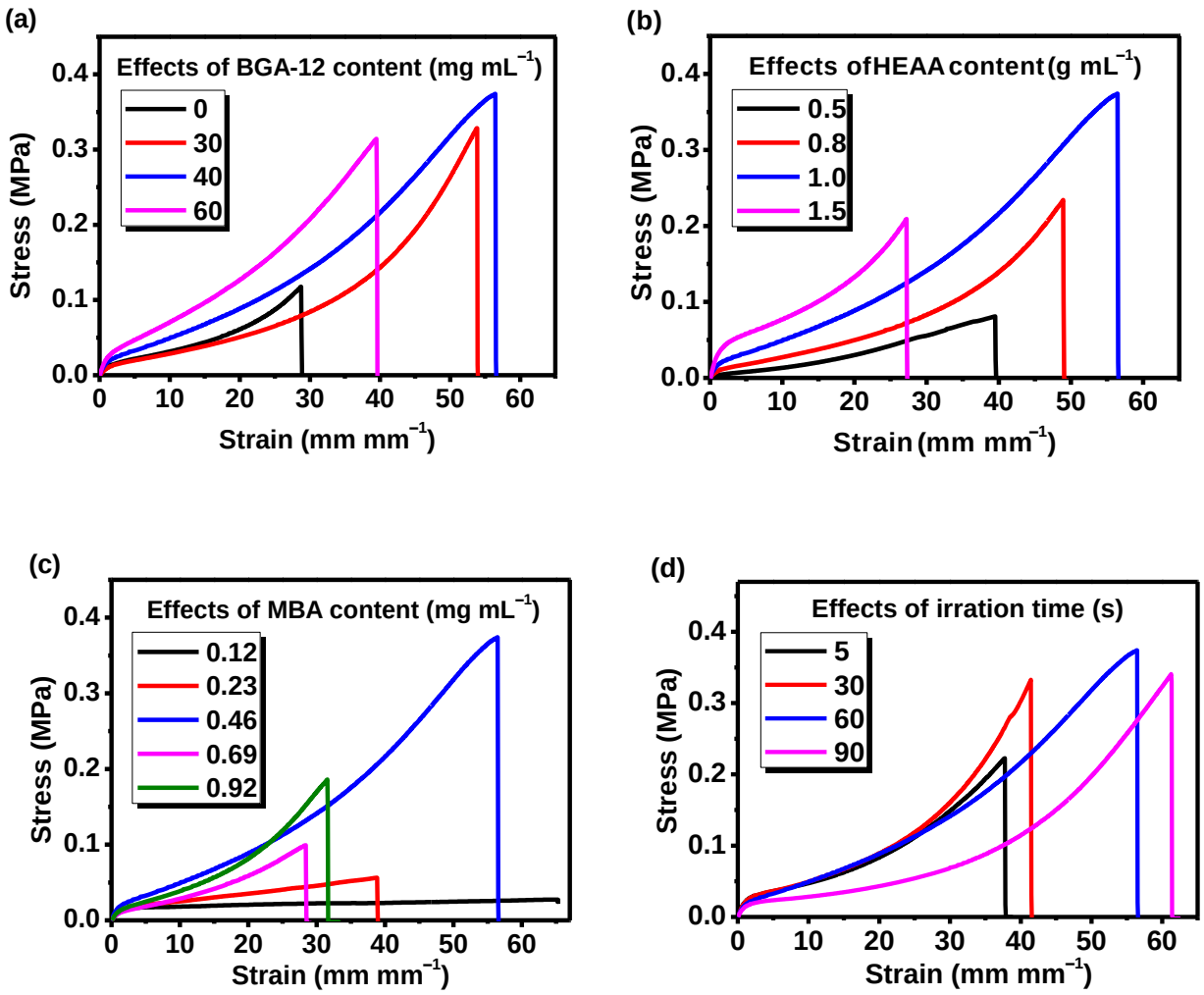

Figure S23. Optimization of the mechanical properties for the BGA-12/PHEAA SP-DN eutectogel. Tensile stress-strain curves of the BGA-12/PHEAA SP-DN eutectogel with varied content of (a) BGA-12 concentration, (b) HEAA concentration, (c) MBA concentration and (d) irradiation time of the UV lamp.

Firstly, we conducted a series of tensile test to examine the effects of BGA-12, HEAA and MBA concentration, as well as the irradiation time of the UV lamp on the mechanical properties of the BGA-12/PHEAA SP-DN eutectogel. As shown in Tables S4-S7 and Figure S23, it is apparent that the mechanical properties of the BGA-12/PHEAA SP-DN eutectogel varied significantly with the increasing of the BGA-12 concentrations. At BGA-12 of 40.0 mg mL^{-1}, the BGA-12/PHEAA SP-DN

eutectogel reached the best tensile property (tensile fracture stress: 0.37 MPa; tensile fracture strain: 56.5 mm mm^{-1}, work of extension at fracture: 8.8 MJ m^{-3}). In Figure S23b, the increase of HEAA content from 0.5 to 1.0 g mL^{-1} enhances the tensile properties of the SP-DN eutectogel, arising from the increased density of polymer chains. Further increasing the HEAA content to 1.5 g mL^{-1} resulted to the deterioration of the tensile properties, which may break the matched balance between supramolecular and polymer networks. As the concentrations of MBA increased from 0.12 to 0.23 mg mL^{-1}, the tensile strength of the SP-DN eutectogel further increased, whereas the stretchability decreased dramatically, showing a competitive equilibrium between the tensile strength and stretchability. At MBA concentration of 0.46 mg mL^{-1}, the BGA-12/PHEAA SP-DN eutectogel reached the best tensile property. It should be pointed out that the BGA-12/PHEAA SP-DN eutectogel exhibits instant *in situ* photopolymerization gelation capacities. It takes only 5 s of UV irradiation (0.4 W cm^{-2}) to obtain a relatively robust SP-DN eutectogel with tensile fracture stress of 0.22 MPa and tensile fracture strain of 37.8 mm mm^{-1}, which even superior to those of PHEAA single-network eutectogel by UV-irradiation of 60 s (0.12 MPa and 28.7 mm mm^{-1}, respectively). Upon irradiating of 60 s or more, the tensile fracture stress and tensile fracture strain of the obtained the BGA-12/PHEAA SP-DN eutectogel no longer rise rapidly but stabilize at a certain level. Based on the results mentioned above, unless otherwise stated, the optimal conditions in the process of synthesizing the BGA-12/PHEAA SP-DN eutectogel for the test samples of 2 mm thickness are BGA-12 of 40 mg mL^{-1}, HEAA of 1.0 g mL^{-1}, MBA of 0.46 mg mL^{-1} and UV-irradiation time of 60 s.

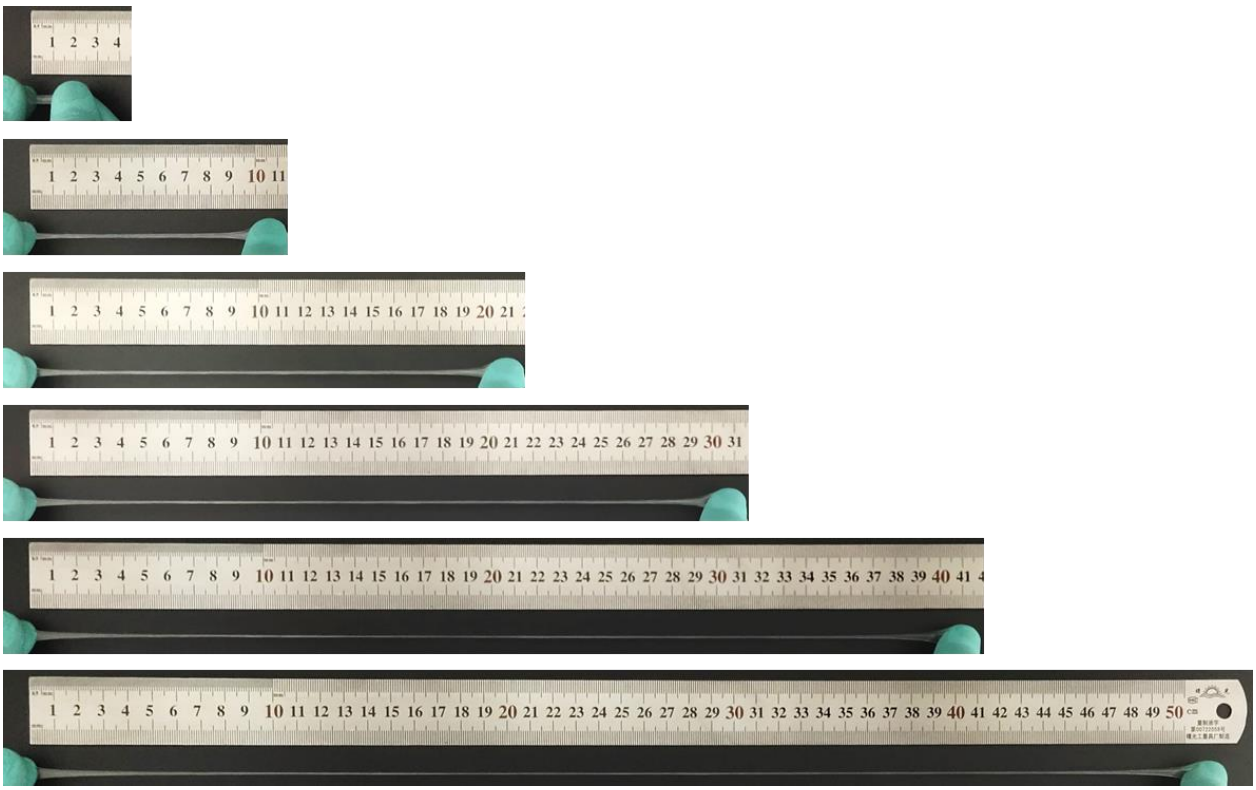

Figure S24. Uniaxial tension performance of the SP-DN eutectogel. A test sample of the BGA-12/PHEAA SP-DN eutectogel with the length of 1.0 cm can be easily stretched to over 50 cm, showing more than 50 times of tensile elongation.

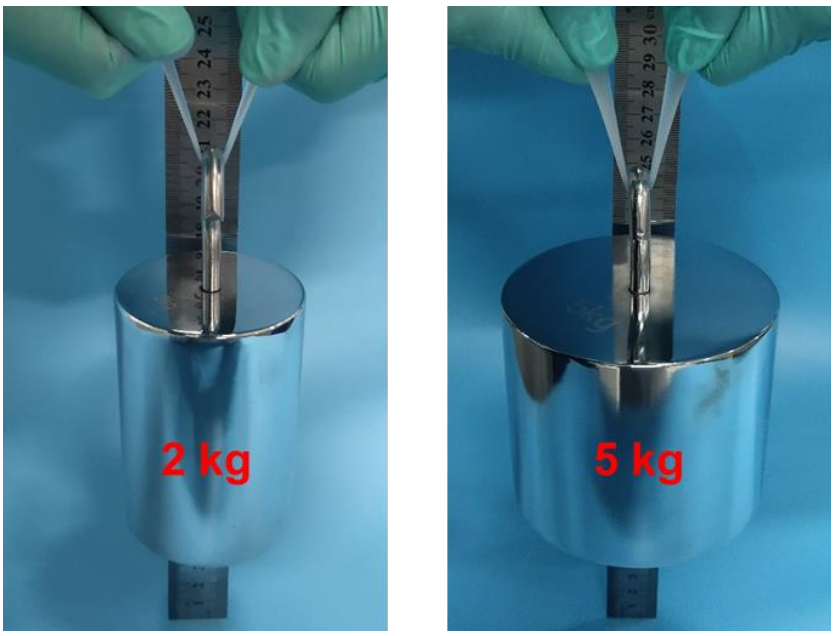

Figure S25. Load-bearing capacity of the SP-DN eutectogel. A test sample of cylindrical BGA-12/PHEAA SP-DN eutectogel with a diameter of 5.0 or 10.0 mm can easily sustain a weight of 2 or 5 kg, respectively, demonstrating a high toughness.

Table S8. Comparison for mechanical properties of the BGA-12/PHEAA SP-DN eutectogel with other double-network gels reported in the literature.

Composition	Tensile fracture stress (MPa)	Tensile fracture strain (mm mm^{-1})	Work of extension at fracture (MJ m^{-3})	Refs.
BGA-12/PHEAA SP-DN eutectogel	**0.37**	**56.5**	**8.8**	**This work**
G4 ~~K~~$^{+}$/PDMAAm hydrogel	0.273	17.62	3.23	8
La-cholate/PAAm hydrogel	0.314	29.85	5.678	9
P(NaSS-co-MPTC) polyampholyte hydrogel	0.1–2.0	1.5–15	0.1–7.0	10
Agar/HPAAm DN hydrogel	0.75	34	–	11
Alginate/polyacrylamide hydrogel	0.156	23	–	12
Bulk agar/pHEAA hydrogel	2.6	8	–	13
Chitosan/PAM hydrogels	5.6	< 0.45	–	14
PAMPS/PAAm hydrogel	17.2	0.92	–	15

Section S5 Adhesiveness of the BGA-12/PHEAA supramolecular-polymer double-network (SP-DN) eutectogel

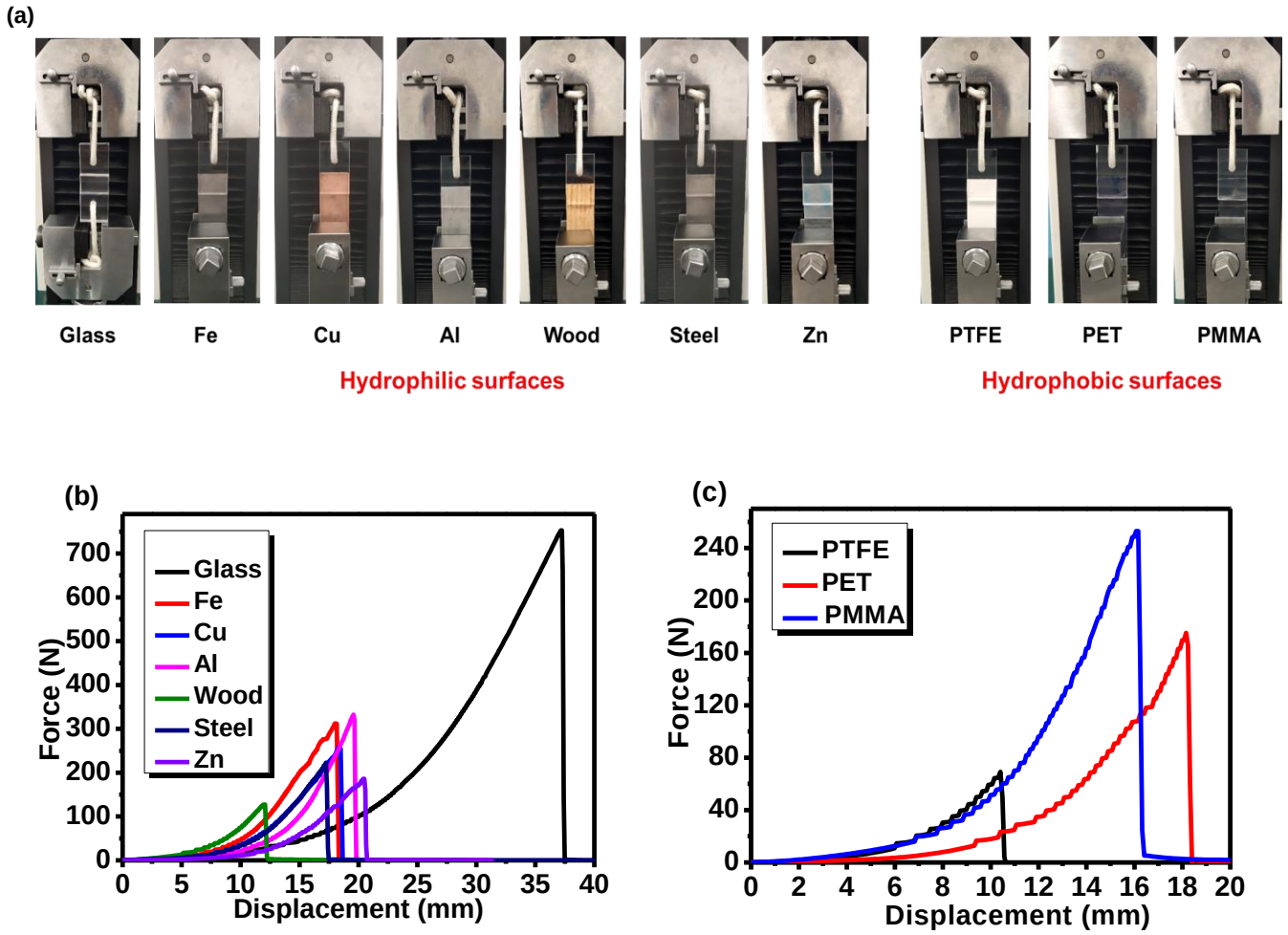

Figure S26. Lap-shear test of the BGA-12/PHEAA SP-DN eutectogel based on different substrates. (a) Experimental photos of the lap-shear test based on different substrates. Force-displacement curves of (b) hydrophilic and (c) hydrophobic substrates, respectively.

Table S9. Comparison for adhesion strength (MPa) with previously reported adhesives determined by lap-shear test.

Adhesives	Adhesion strength (MPa)						Underwater *in situ* adhesion on glass	Tempe-rature range (°C)	Refs.
	Hydrophilic substrates			Hydrophobic substrates					
	Glass	Metal plates	Wood	PMMA	PET	PTFE			
BGA-12/PHEAA SP-DN eutectogel	**1.25**	**0.55 for Al 0.52 for Fe 0.43 for Cu 0.37 for steel 0.31 for Zn**	**0.21**	**0.42 for PMMA**	**0.29 for PET**	**0.12 for PTFE**	**0.47**	**–196 to 200**	**This work**
gelatin organohydrogel	~0.12	0.15 for Cu	–	~0.1 for PET			–	–70 to RT[a]	16
PAAm/PVA/CS/ $FeCl_3$/TCNF organohydrogel	< 0.003	–	–	< 0.006 for PMMA	< 0.004 for PTFE		–	–20 to RT[a]	17
PAH/TPP polyelectrolytes gels	–	–	–	–			0.435	RT[a]	18
polyampholyte hydrogel	–	–	–	–			< 0.015	RT[a]	19
polyzwitterion/ clay nanocomposite hydrogels	< 0.04	–	<0.03	< 0.005 for PMMA	< 0.015 for PET		–	RT[a]	20
PVA exogel	0.30	0.10 for Al	–	0.18 for PMMA			–	RT[a]	21
cellulose nanocomposite hydrogel	~0.07	~ 0.07 for Al	~0.12	~ 0.05 for PTFE			–	RT[a]	22
poly(AAm-*co*-AAc)/PDADMAC hydrogel	~0.008	~0.006 for Steel	–	~0.007 for PMMA			–	RT[a]	23
(PDA-clay-PAM) hydrogel	0.12	0.808 for Ti	–	0.807 for polyethylene (PE)			–	RT[a]	24

[a] RT = room temperature

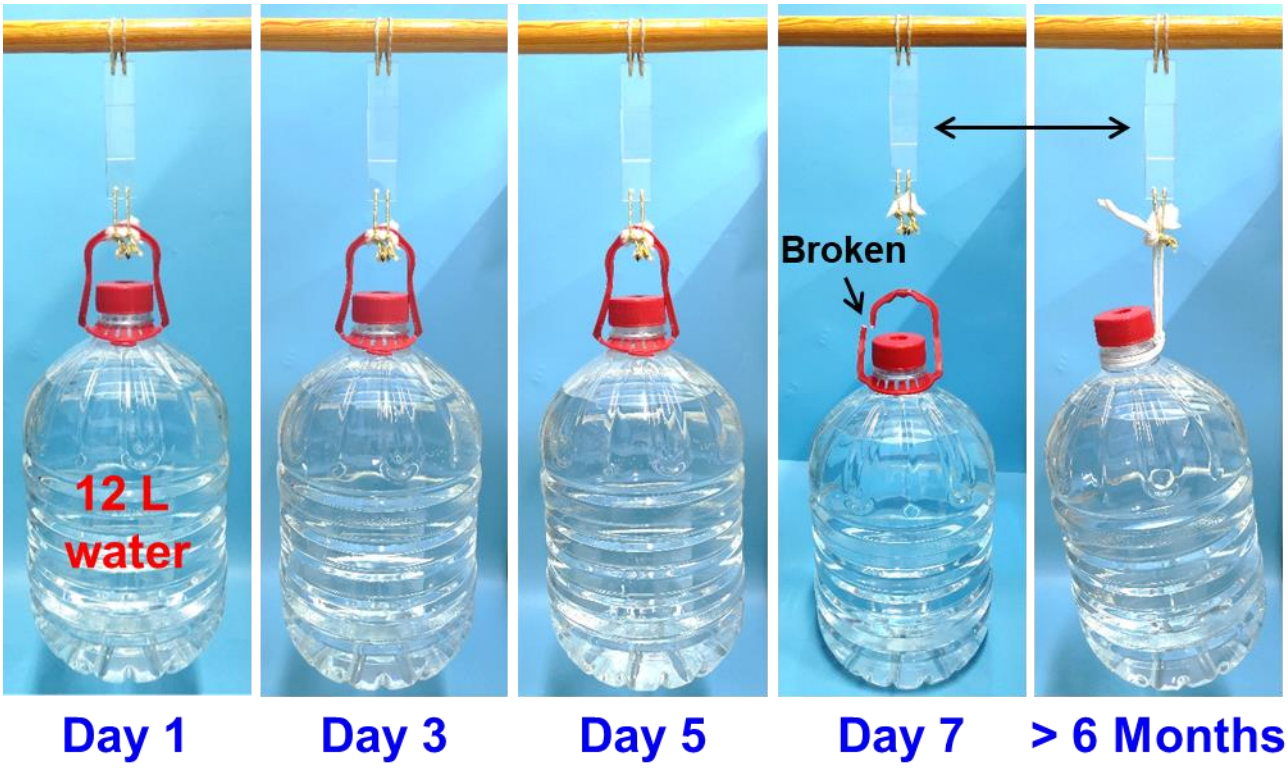

Figure S27. Long-term adhesion of the SP-DN eutectogel between glass plates. Loading test (>12 kg) of long-lasting adhesiveness of the BGA-12/PHEAA SP-DN eutectogel between glass plates. According to our test results, on the 7th day, the red plastic handle of the mineral water bucket (~12 L) had broken. Afterwards, the BGA-12/PHEAA SP-DN eutectogel between glass plates still maintains excellent adhesion for over 6 months until submitting this manuscript.

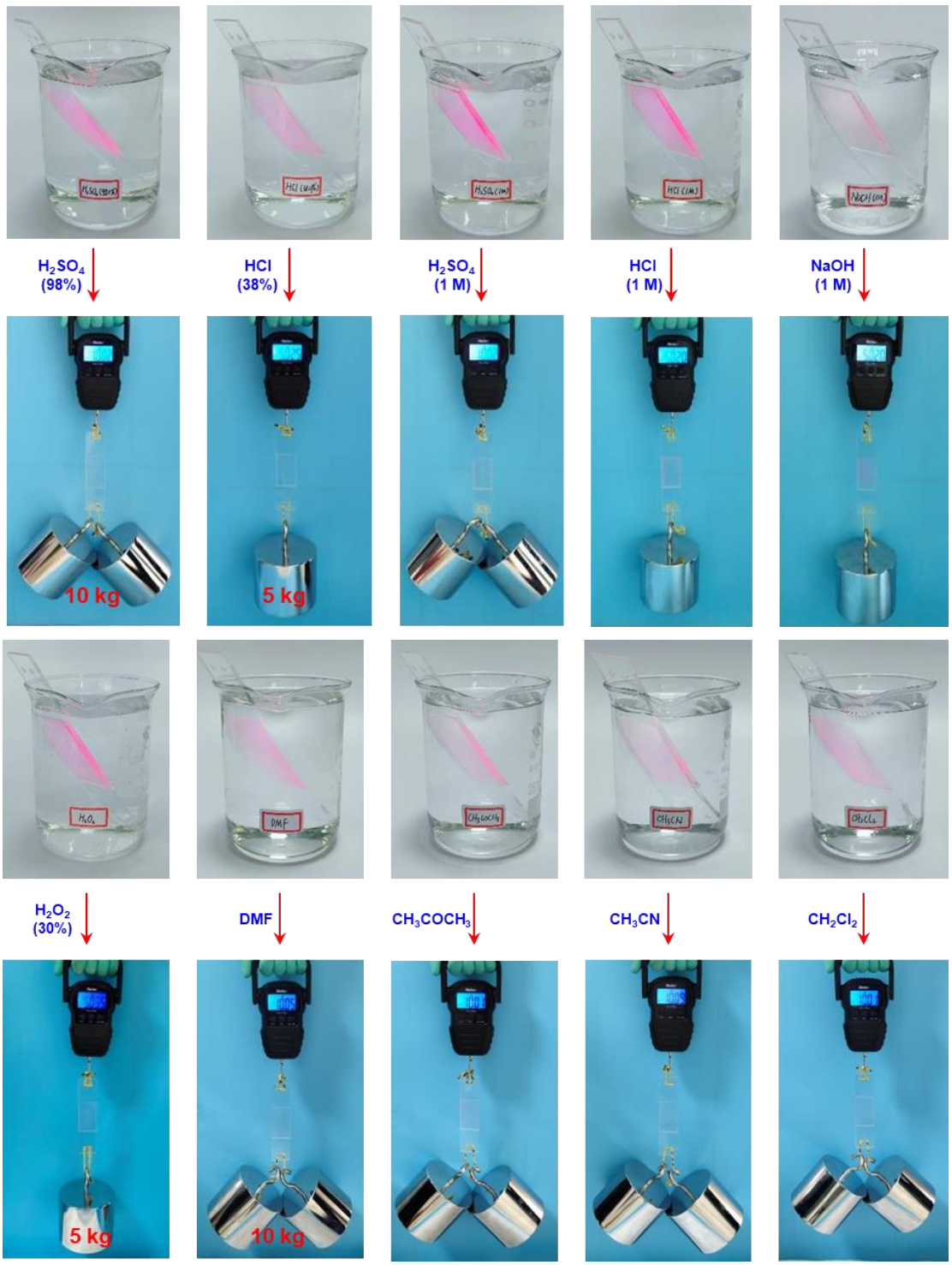

Figure S28. Solvent-resistant adhesion of the BGA-12/PHEAA SP-DN eutectogel evaluated by macroscopic test. Adhesiveness and loading test (5 or 10 kg) of the BGA-12/PHEAA SP-DN eutectogel between glass plates, being immersed in various strong and weak acids and bases with different concentrations as well as common organic solvents, after at least 24 h, demonstrating the excellent solvent-resistant adhesiveness. Red dyes of rhodamine B were added to visually observe the SP-DN eutectogel.

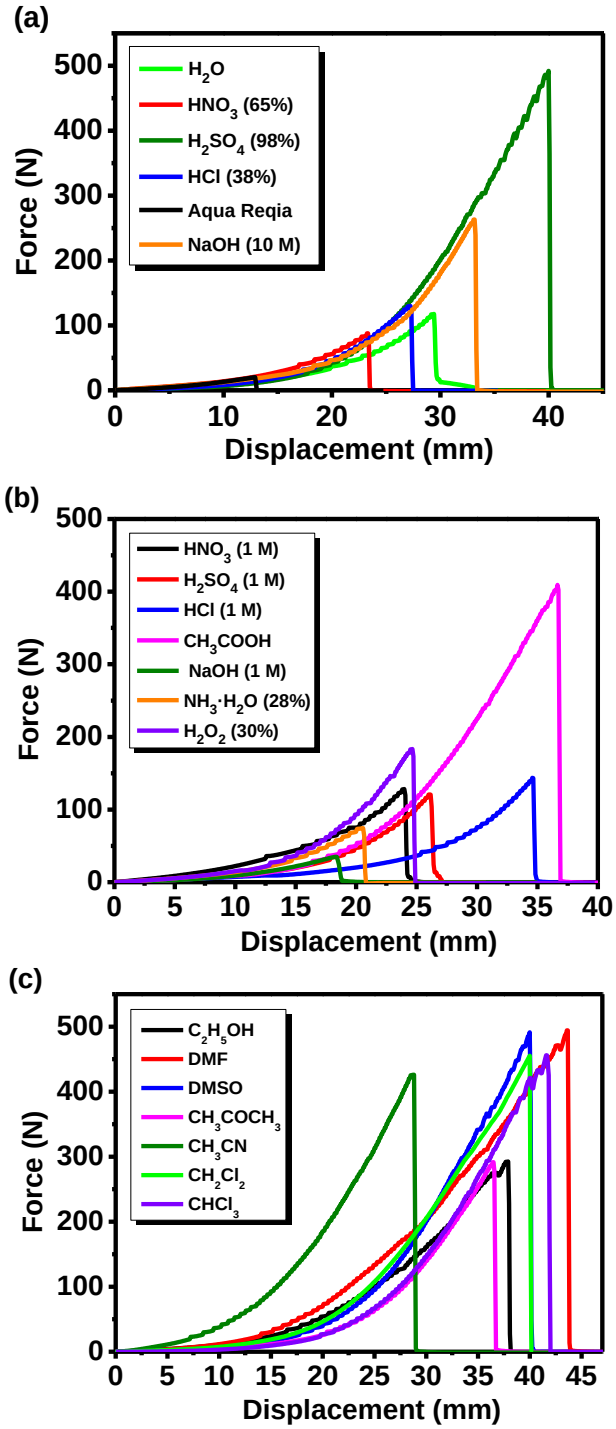

Figure S29. Solvent-resistant adhesion of the BGA-12/PHEAA SP-DN eutectogel evaluated by lap-shear test. Lap-shear test curves of the BGA-12/PHEAA SP-DN eutectogel between glass plates after being immersed in (a) concentrated acid and bases, (b) diluted acids and bases and (c) common organic solvents after at least 24 h, respectively. The adhesion strengths still kept as 0.15–0.82 MPa for concentrated acid and bases system, 0.12–0.68 MPa for diluted acid and bases system and 0.50–0.80

MPa for organic solvents system. The samples in aqua regia and 1 M NaOH showed relative weak adhesion strength (< 0.10 MPa).

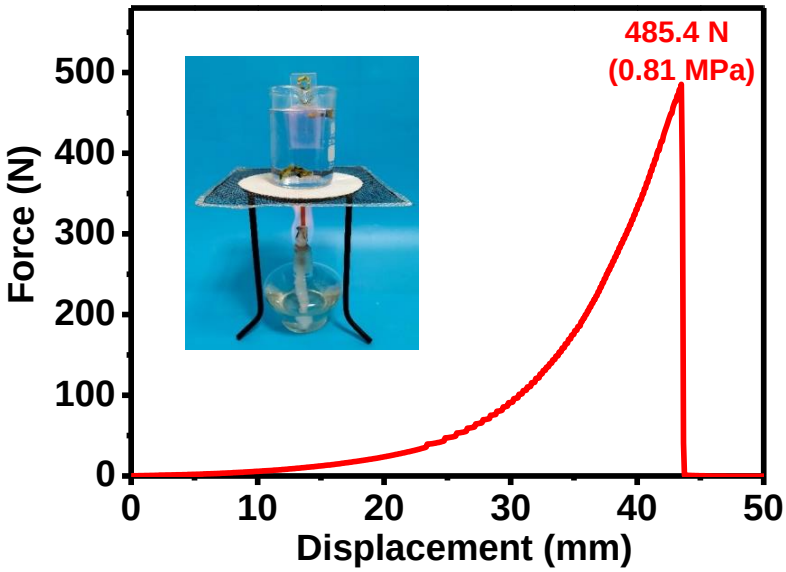

Figure S30. Boiling water-resistant adhesion of the BGA-12/PHEAA SP-DN eutectogel. Lap-shear test curve of the BGA-12/PHEAA SP-DN eutectogel between glass plates after being immersed in boiling water (100 ^{o}C) over 1 h. Inset: Experimental photo of the boiling water-resistant adhesion test.

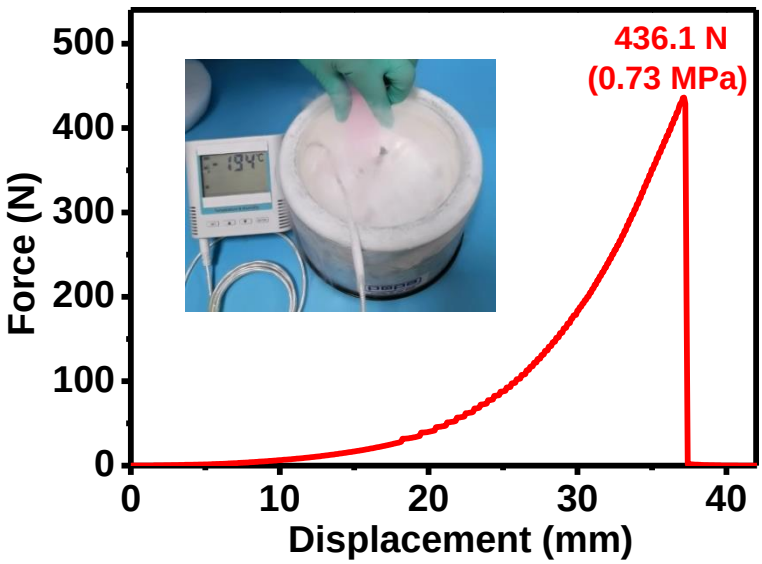

Figure S31. Ultra-low temperature resistant adhesion of the BGA-12/PHEAA SP-DN eutectogel. Lap-shear test curve of the BGA-12/PHEAA SP-DN eutectogel between glass plates after being immersed in liquid nitrogen (–196 ^{o}C) for over 1 h. Inset: Experimental photo of the prepared sample for loading test in Figure 5b of the main text. Red dyes of rhodamine B were added to visually observe the SP-DN eutectogel.

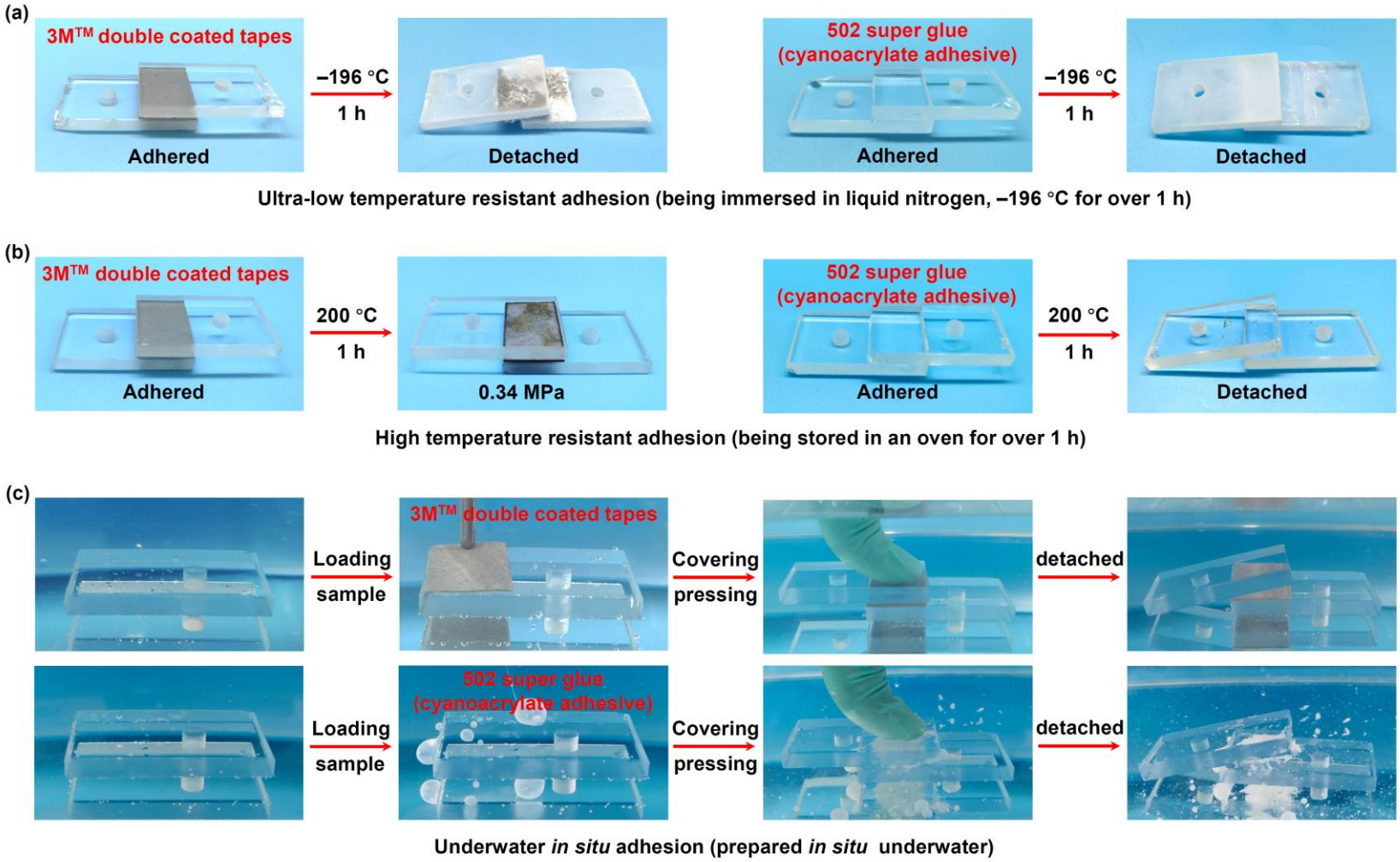

Figure S32. Adhesiveness of representative commercial adhesives under extreme conditions. Experimental photo of 502 super glue (a cyanoacrylate adhesive) and 3M^{TM} double coated tapes: (a) after being immersed in ultra-low temperature liquid nitrogen (–196 ^{o}C) for over 1 h, (b) after being placed in an oven (200 ^{o}C) for over 1 h and (c) after being tested *in situ* underwater.

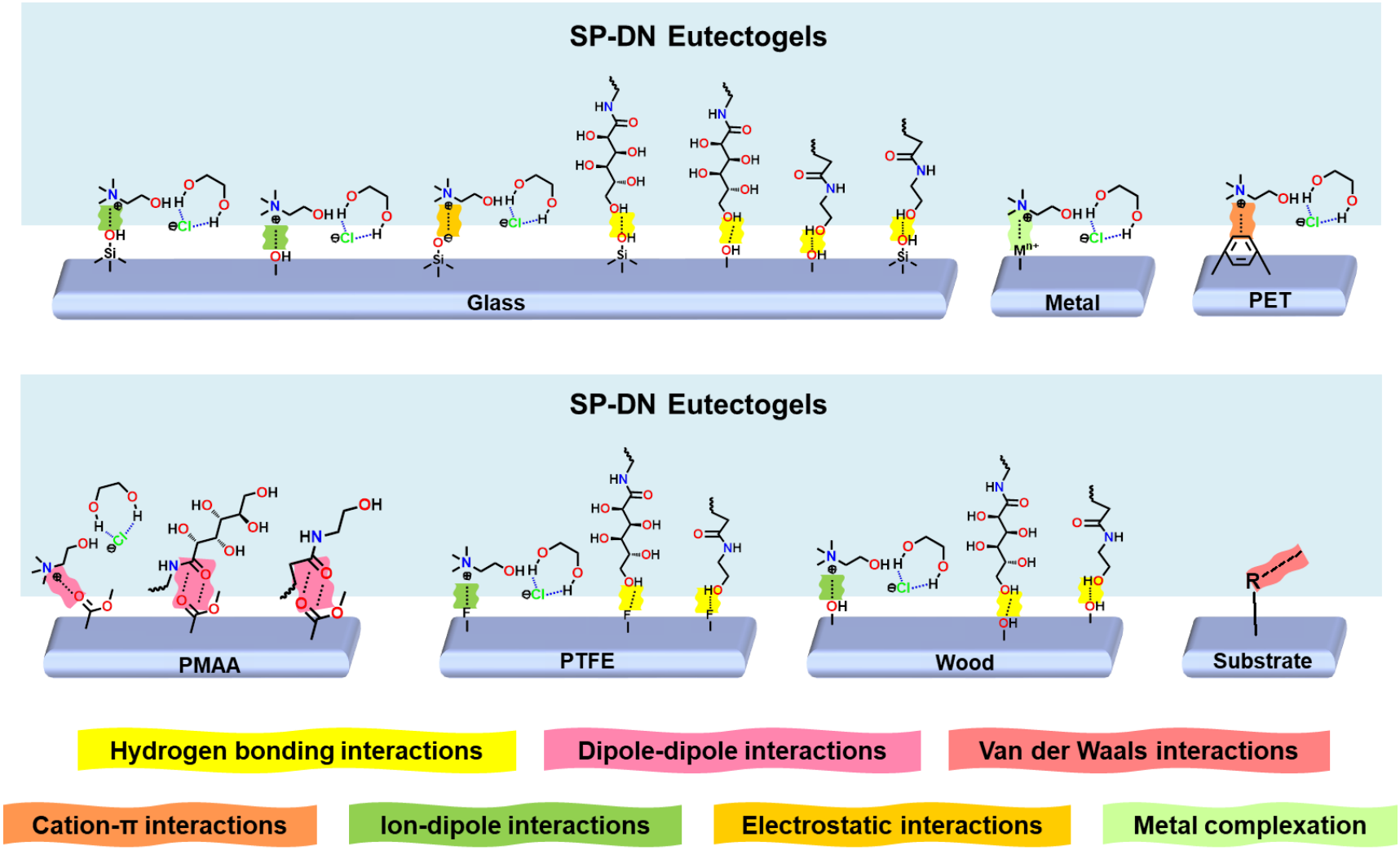

Figure S33. The possible interfacial interactions between the SP-DN eutectogels and different substrates.

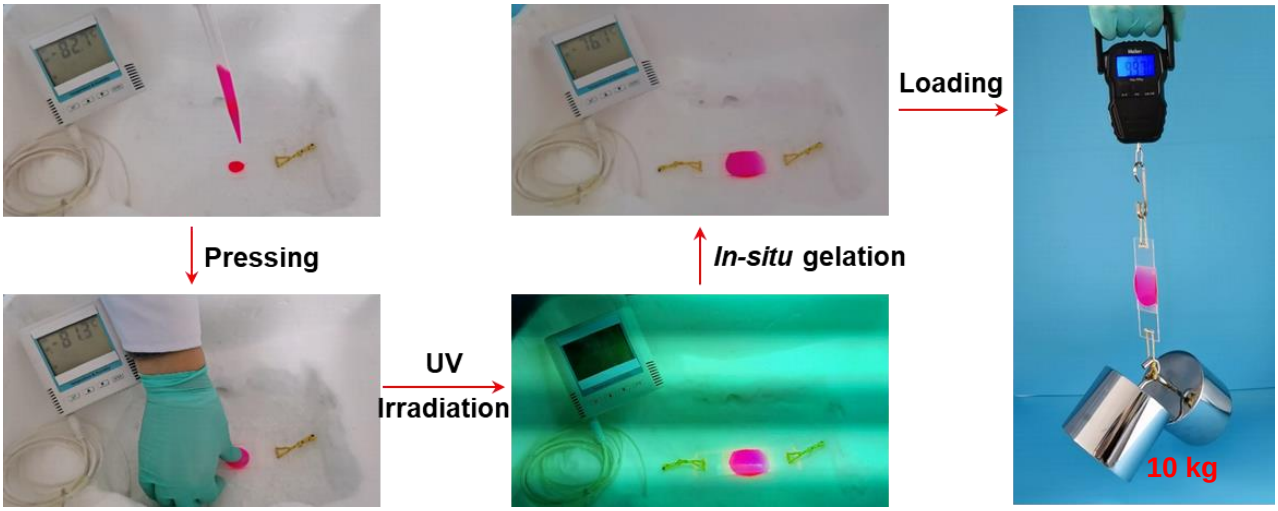

Figure S34. Ultra-low temperature (dry-ice environment, approximately –80 °C) *in situ* adhesiveness of the BGA-12/PHEAA SP-DN eutectogel. Preparation process and loading test (10 kg) of the adhered glass prepared *via in situ* photopolymerization of BGA-12/PHEAA SP-DN eutectogel under approximately –80 °C (~5 s). Red dyes of rhodamine B were added to visually observe the SP-DN eutectogel.

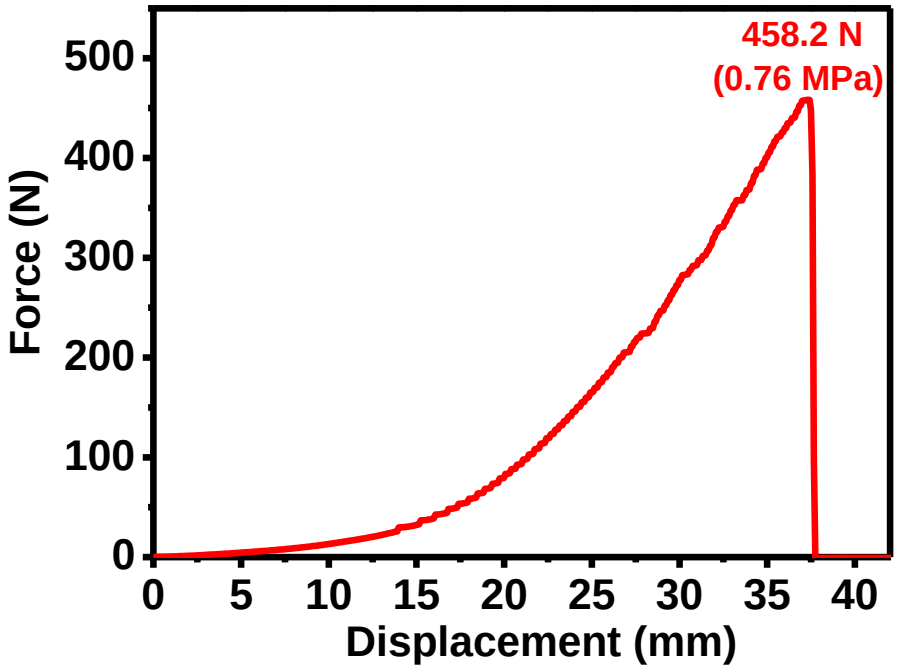

Figure S35. Lap-shear test curve of the BGA-12/PHEAA SP-DN eutectogel adhered glass prepared by *in situ* photopolymerization under approximately –80 °C.

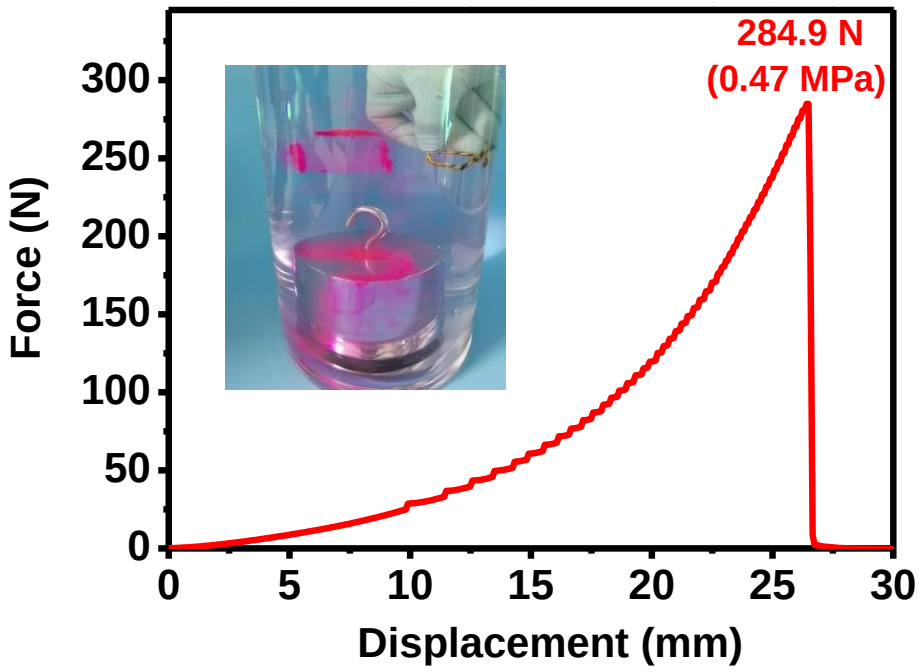

Figure S36. Underwater *in situ* adhesiveness of the BGA-12/PHEAA SP-DN eutectogel. Lap-shear test curve of the BGA-12/PHEAA SP-DN eutectogel between glass plates prepared by photopolymerization underwater *in situ* (~5 s). Inset: experimental site photo of the prepared sample for loading test in Figure 5c in the main text. Red dyes of rhodamine B were added to visually observe the SP-DN eutectogel.

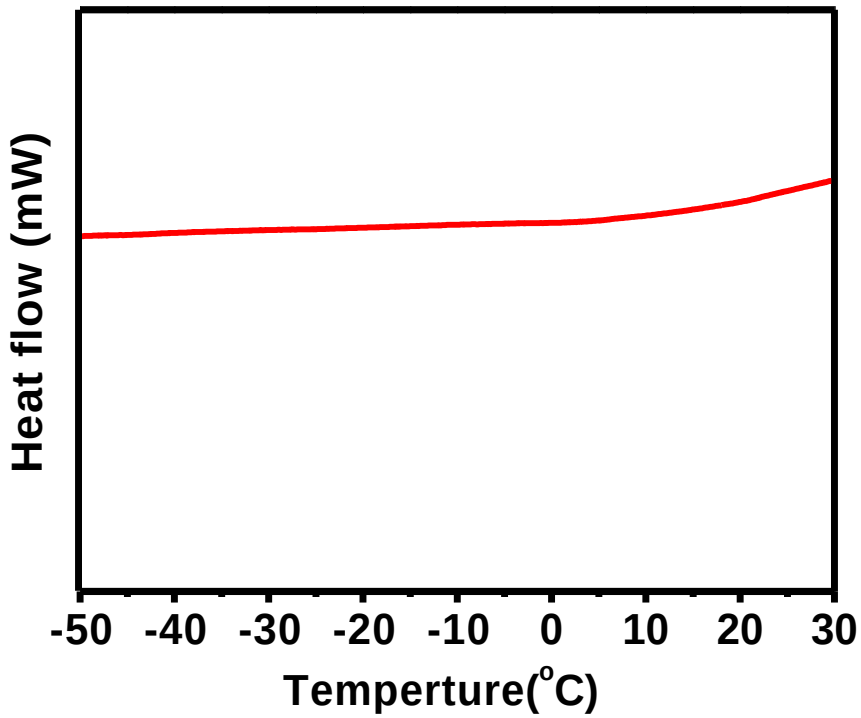

Figure S37. DSC curve of the SP-DN eutectogel.

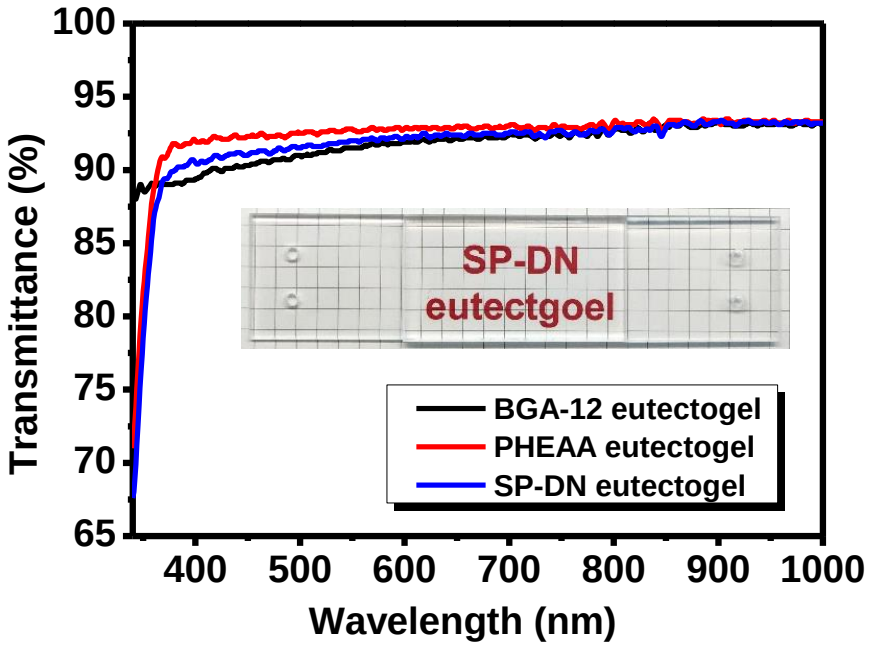

Figure S38. Transparency of the prepared eutectogels. The transmittanc of BGA-12, PHEAA and BGA-12/PHEAA SP-DN eutectogel coating layers between glass plates (Inset: photo for the BGA-12/PHEAA SP-DN eutectogel coating layer between glass plates).

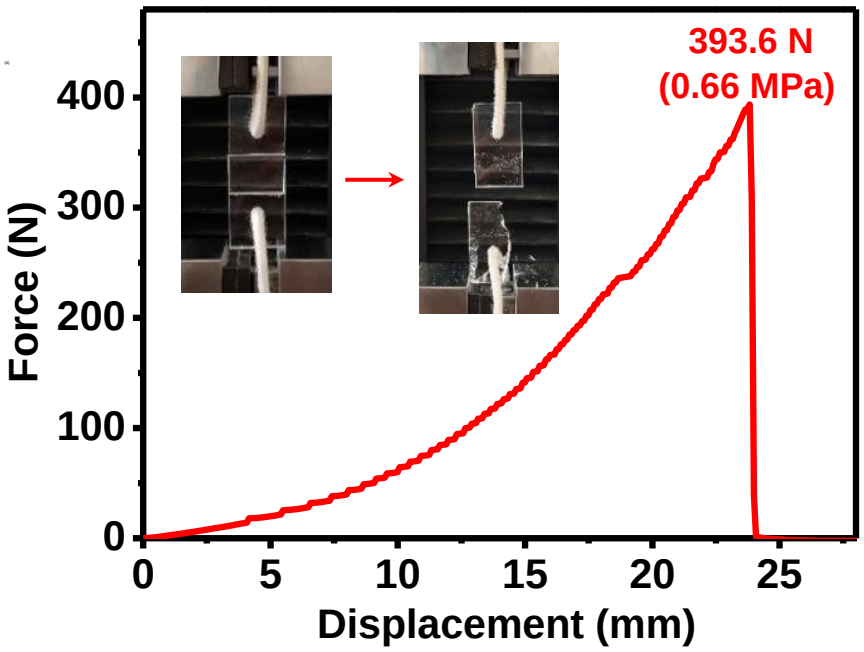

Figure S39. Ultrafast *in situ* adhesiveness of the BGA-12/PHEAA SP-DN eutectogel. Lap-shear test curve of the BGA-12/PHEAA SP-DN eutectogel between glass plates by a very short UV-irradiation time (~3 s). Inset: experimental site photo of the sample before and after lap-shear test.

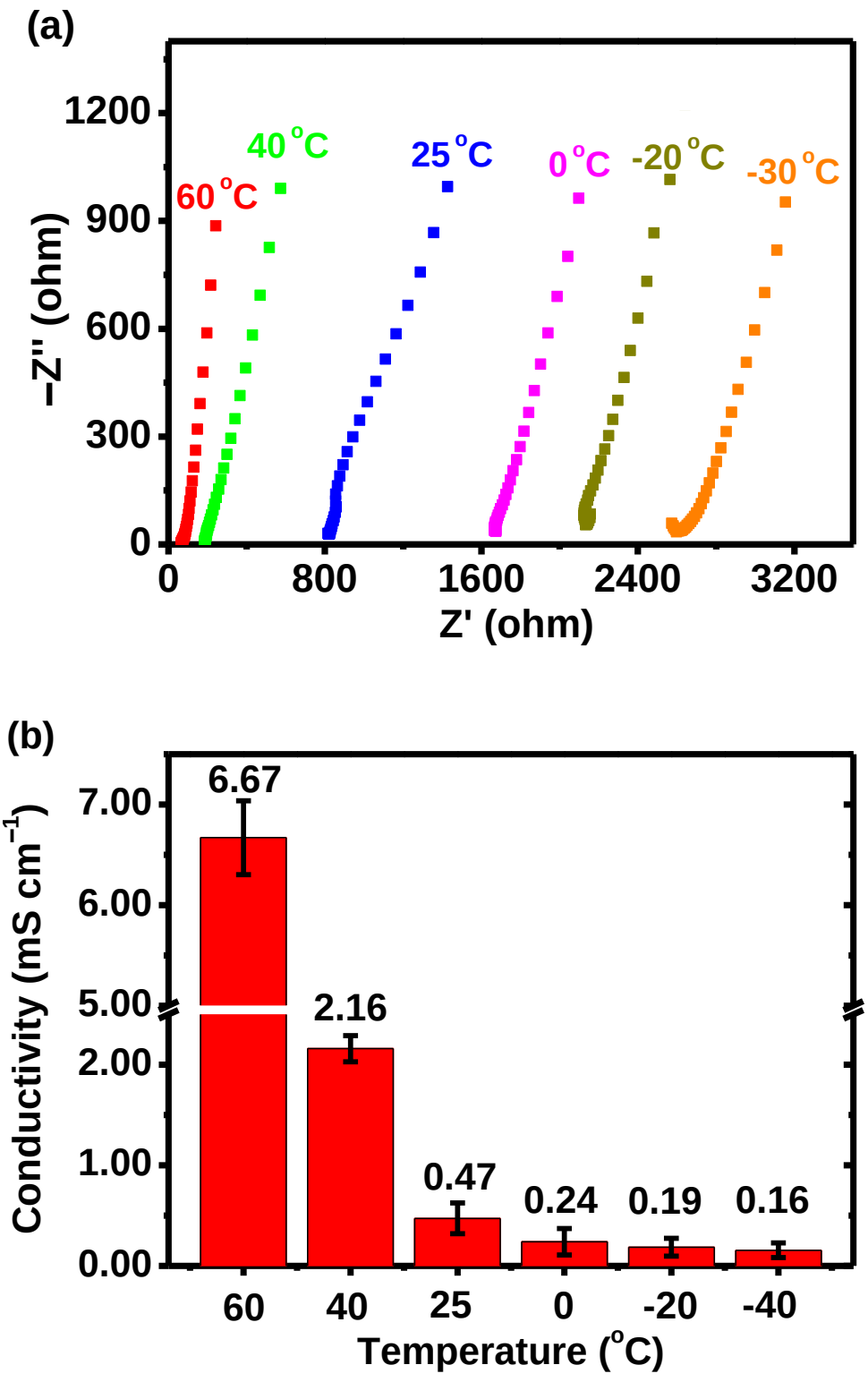

Figure S40. Conductivity of the BGA-12/PHEAA SP-DN eutectogel. The EIS plot (a) and the corresponding conductivity (b) of the BGA-12/PHEAA SP-DN eutectogel at various temperatures. Error bars represent standard deviations of data collected from at least three separate samples.

Section S6 Rreferences

S1. Chen, Q. et al. Simultaneous Enhancement of Stiffness and Toughness in Hybrid Double-Network Hydrogels *via* the First, Physically Linked Network. *Macromolecules* **48**, 8003−8010 (2015).

S2. Hu, J. et al. Microgel-Reinforced Hydrogel Films with High Mechanical Strength and Their Visible Mesoscale Fracture Structure. *Macromolecules* **44**, 7775−7781 (2011).

S3. Troć, A., Gajewy, J., Danikiewicz, W. & Kwit, M. Specific Noncovalent Association of Chiral Large-Ring Hexaimines: Ion Mobility Mass Spectrometry and PM7 Study. *Chem. Eur. J.* **22**, 13258−13264 (2016).

S4. Stewart, J.J.P. Optimization of parameters for semiempirical methods VI: more modifications to the NDDO approximations and re-optimization of parameters. *J. Mol. Model.* **19**, 1−32 (2013).

S5. Grimme, S., Ehrlich, S. & Goerigk, L. Effect of the Damping Function in Dispersion Corrected Density Functional Theory. *J. Comput. Chem.* **32**, 1456−1465 (2011).

S6. Frisch, M. J.; Trucks, G. W.; Schlegel, H. B.; Scuseria, G. E.; Robb, M. A.; Cheeseman, J. R.; Scalmani, G.; Barone, V.; Petersson, G. A.; Nakatsuji, H.; Li, X.; Caricato, M.; Marenich, A. V.; Bloino, J.; Janesko, B. G.; Gomperts, R.; Mennucci, B.; Hratchian, H. P.; Ortiz, J. V.; Izmaylov, A. F.; Sonnenberg, J. L.; Williams-Young, D.; Ding, F.; Lipparini, F.; Egidi, F.; Goings, J.; Peng, B.; Petrone, A.; Henderson, T.; Ranasinghe, D.; Zakrzewski, V. G.; Gao, J.; Rega, N.; Zheng, G.; Liang, W.; Hada, M.; Ehara, M.; Toyota, K.; Fukuda, R.; Hasegawa, J.; Ishida, M.; Nakajima, T.; Honda, Y.; Kitao, O.; Nakai, H.; Vreven, T.; Throssell, K.; Montgomery, J. A.; Jr., Peralta, J. E.; Ogliaro, F.; Bearpark, M. J.; Heyd, J. J.; Brothers, E. N.; Kudin, K. N.; Staroverov, V. N.; Keith, T. A.; Kobayashi, R.; Normand, J.; Raghavachari, K.; Rendell, A. P.; Burant, J. C.; Iyengar, S. S.; Tomasi, J.; Cossi, M.; Millam, J. M.; Klene, M.; Adamo, C.; Cammi, R.; Ochterski, J. W.; Martin, R. L.; Morokuma, K.; Farkas, O.; Foresman, J. B.; Fox, D. J. Gaussian 16, Revision A.03; Gaussian, Inc.: Wallingford, CT, 2016.

S7. Legault, C. Y. CYLview, 1.0b; Université de Sherbrooke, 2009 (http://www.cylview.org).

S8. Chen, F. et al. General Strategy To Fabricate Strong and Tough Low-Molecular-Weight Gelator-Based Supramolecular Hydrogels with Double Network Structure. *Chem. Mater.* **30**, 1743−1754 (2018).

S9. Chen, F. et al. Fabrication and mechanical behaviors of novel supramolecular/polymer hybrid double network hydrogels. *Polymer* **168**, 159−167 (2019).

S10. Sun, T.L. et al. Physical hydrogels composed of polyampholytes demonstrate high toughness and viscoelasticity. *Nat. Mater.* **12**, 932−937 (2013).

S11. Wang, Y. et al. A Highly Elastic and Reversibly Stretchable All-Polymer Supercapacitor. *Angew. Chem. Int. Ed.* **58**, 15707−15711 (2019).

S12. Sun, J.Y. et al. Highly stretchable and tough hydrogels. *Nature* **489**, 133−136 (2012).

S13. Chen, H. et al. Super Bulk and Interfacial Toughness of Physically Crosslinked Double-Network Hydrogels. *Adv. Funct. Mater.* **27**, 1703086 (2017).

S14. Yang, Y., Wang, X., Yang, F., Wang, L. & Wu, D. Highly Elastic and Ultratough Hybrid Ionic-Covalent Hydrogels with Tunable Structures and Mechanics. *Adv. Mater.* **30**, e1707071 (2018).

S15. Gong, J.P., Katsuyama, Y., Kurokawa, T. & Osada, Y. Double-Network Hydrogels with Extremely High Mechanical Strength. *Adv. Mater.* **15**, 1155−1158 (2003).

S16. Qin, Z. et al. Freezing-Tolerant Supramolecular Organohydrogel with High Toughness, Thermoplasticity, and Healable and Adhesive Properties. *ACS Appl. Mater. Interfaces* **11**, 21184−21193 (2019).

S17. You, Z. et al. One-pot synthesis of multi-functional cellulose-based ionic conductive organohydrogel with low-temperature strain sensitivity. *Carbohydr. Polym.* **251**, 117019 (2021).

S18. Huang, Y., Lawrence, P.G. & Lapitsky, Y. Self-Assembly of Stiff, Adhesive and Self-Healing Gels from Common Polyelectrolytes. *Langmuir* **30**, 7771−7777 (2014).

S19. Rao, P. et al. Tough Hydrogels with Fast, Strong, and Reversible Underwater Adhesion Based on a Multiscale Design. *Adv. Mater.* **30**, 1801884 (2018).

S20. Gao, G. et al. Bioinspired Self-Healing Human-Machine Interactive Touch Pad with Pressure-Sensitive Adhesiveness on Targeted Substrates. *Adv. Mater.* 2004290 (2020).

S21. Xu, L. et al. A Solvent-Exchange Strategy to Regulate Noncovalent Interactions for Strong and Antiswelling Hydrogels. *Adv. Mater.* 2004579 (2020).

S22. Shao, C. et al. Mimicking Dynamic Adhesiveness and Strain-Stiffening Behavior of Biological Tissues in Tough and Self-Healable Cellulose Nanocomposite Hydrogels. *ACS Appl. Mater. Interfaces* **11**, 5885−5895 (2019).

S23. Li, W. et al. Polyelectrolyte-based physical adhesive hydrogels with excellent mechanical properties for biomedical applications. *J. Mater. Chem. B* **6**, 4799−4807 (2018).

S24. Han, L. et al. Mussel-Inspired Adhesive and Tough Hydrogel Based on Nanoclay Confined Dopamine Polymerization. *ACS Nano* **11**, 2561−2574 (2017).